Inorganic Chemistry

Article

pubs.acs.org/IC

Heteroleptic Dipyrrinato Complexes Containing 5-Ferrocenyldipyrromethene and Dithiocarbamates as Coligands: Selective Chromogenic and Redox Probes

Rakesh Kumar Gupta,[†] Rampal Pandey,[†] Roopshikha Singh,[†] Nitin Srivastava,[†] Biswajit Maiti,[†] Satyen Saha,[†] Peizhou Li,[‡] Qiang Xu,[‡] and Daya Shankar Pandey*[,†]

[†]Department of Chemistry, Faculty of Science, Banaras Hindu University, Varanasi-221 005 (U.P.), India

[‡]National Institute of Advanced Industrial Science and Technology (AIST), 1-8-31, Midorigaoka, Ikeda, Osaka 563-8577, Japan

Supporting Information

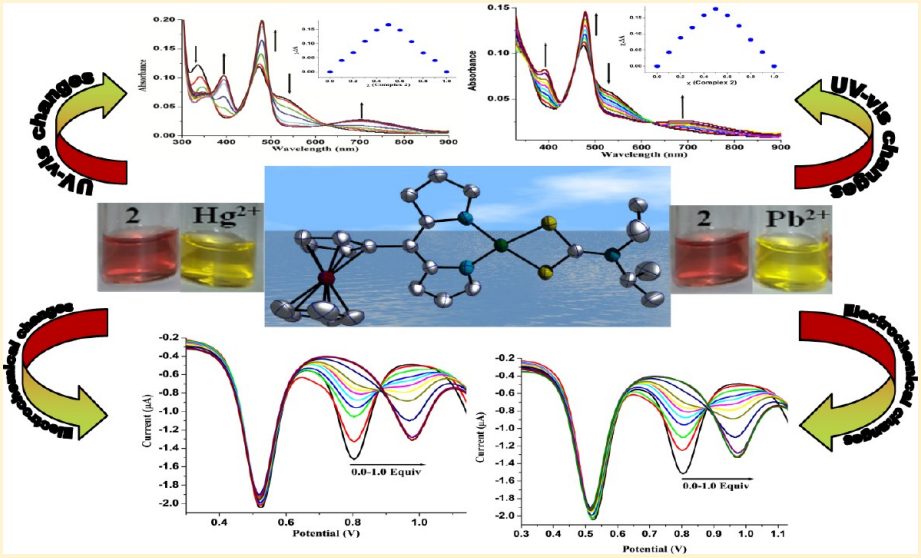

ABSTRACT: Six heteroleptic dipyrrinato complexes [Ni(fcdpm)(dedtc)] (**1**), [Ni(fcdpm)(dipdtc)] (**2**), [Ni(fcdpm)(dbdtc)] (**3**), [Pd(fcdpm)(dedtc)] (**4**), [Pd(fcdpm)(dipdtc)] (**5**), and [Pd(fcdpm)(dbdtc)] (**6**) (fcdpm = 5-ferrocenyldipyrromethene; dedtc = diethyldithiocarbamate; dipdtc = diisopropyldithiocarbamate; dbdtc = dibutyldithiocarbamate) have been synthesized and characterized by elemental analyses and spectral (ESI-MS, IR, ^{1}H, ^{13}C NMR, UV−vis) and electrochemical studies. Crystal structures of **1**, **2**, **4**, and **5** have been authenticated by X-ray single-crystal analyses. Nickel-based complexes **1**−**3** display selective chromogenic and redox sensing for Hg^{2+} and Pb^{2+} ions, while palladium complexes **4**−**6** display selective chromogenic and redox sensing only for Hg^{2+}. Electronic absorption, ESI-MS, and electrochemical studies indicated that sensing arises from interaction between **1**−**3** and Hg^{2+}/Pb^{2+} through sulfur of the coordinated dithiocarbamates, while it arises from the pyrrolic nitrogen of fcdpm and dithiocarbamate sulfur from **4**−**6** and Hg^{2+}. Different modes of binding between Ni and Pd complexes have further been supported by theoretical studies. The receptor−cation binding constants (K_a) and stoichiometry between probes and Hg^{2+}/Pb^{2+} have been estimated by the Benesi−Hildebrand method and Job's plot analysis. Detection limits for **1**−**3** toward Hg^{2+}/Pb^{2+} and **4**−**6** for Hg^{2+} have been found to be reasonably high.

INTRODUCTION

Heavy and transition metal ions play a significant role in many physiological processes of organisms; therefore, development of highly selective and sensitive tools for their detection is essential.[1] Among these, Hg^{2+} and Pb^{2+} are particularly important due to their high toxicity and severe effect on living organisms.[2] Despite its high toxicity mercury is extensively used in many industrial processes and manufacture of important products.[3] It is distributed in the environment in various forms like elemental (Hg^{0}), inorganic (Hg^{2+}), and organic methyl mercury (CH_3Hg^{+}). Highly soluble and reactive inorganic mercury (Hg^{2+}) can bind to a variety of ligands present in the organisms, particularly those containing a sulfur functionality.[4] Organic methyl mercury (CH_3Hg^{+}) present in the environment easily enters in the tissues of fish and marine animals through the food chain, and their subsequent consumption by human beings can cause damage to kidneys, DNA, skin, respiratory/

Received: May 3, 2012
Published: August 7, 2012

central nervous system, and other organs.[5] Similarly, in the list of toxic substances lead ranks third and causes serious health problems.[6] The pollution encountered by lead is an ongoing threat to human health, particularly in children: it causes memory loss, mental retardation, anemia, muscle paralysis, etc.[7] Considering the toxicity problems associated with Hg^{2+} and Pb^{2+} ions development of techniques for their detection has been a challenging task.[8] Usually methods used for their detection viz. atomic absorption spectrometry and inductively coupled plasma mass spectrometry are expensive, complex, and inappropriate for on-site analyses.[9] To overcome this problem several Hg^{2+} and Pb^{2+} selective chromogenic, fluorogenic, and electrochemical sensors have been devised.[10] Among these, chromogenic sensors have attracted lots of attention owing to their ability to allow naked eye detection in a simple and cost-effective manner.[11] Further, most of the work on selective chemosensors for aforesaid metal ions have been focused on individual optical signaling, multichannel sensors capable of both optical and electrochemical sensing are rather scarce.[6,10,12]

Furthermore, dipyrromethenes (dipyrrins) possessing a conjugated π system form complexes with a variety of metal ions and are extensively involved in self-assembly processes.[13] Among these, meso-substituted dipyrrins and complexes based on it have been interesting because of their fascinating optical properties.[14] As a signaling unit, dipyrrin chromophore consists of many attractive features like sensitivity, ease of signal transduction, and long wavelength characteristics.[13,14] Incorporation of the ferrocenyl unit as a meso substituent in dipyrrins may be interesting in terms of both catalytic properties and intramolecular charge transfer.[15] Ferrocene-based receptors have been promising as these serve as suitable redox-active building blocks and can be easily functionalized and incorporated into numerous structures.[16] Such systems have been useful in electrochemical sensing of cations, anions, and neutral molecules owing to changes in the Fc/Fc^{+} redox couple.[17] Further, dithiocarbamates (dtc) containing sulfur have scarcely been used as a receptor for heavy and transition metal ions. It is well known that soft metal ions like Hg^{2+} and Pb^{2+} preferentially interact with sulfur.[18] Inclusion of sulfur into a ligand or complex may enable the ensuing system to interact with soft metal ions, change their photophysical properties, and form the basis for their detection.[19]

In a continuation of studies on the synthetic, structural, and photophysical properties of homo/heteroleptic dipyrrinato complexes and to investigate the applicability of complexes containing both fcdpm and various dithiocarbamates in multichannel sensing of Hg^{2+} and Pb^{2+} ions an entirely new series of heteroleptic dipyrrinato complexes **1**−**6** has been prepared and fully characterized.[20] In these complexes the dithiocarbamates possessing soft sulfur sites have been chosen as auxiliary ligands and 5-ferrocenyldipyrromethene as the signaling unit. In the present study we focused our attention mainly on Ni(II) and Pd(II) (d^8) systems as these preferentially form square planar heteroleptic dipyrrinato complexes and may offer suitable sites for interaction with cations/anions over other geometries. Further, Pd(II) systems were chosen to investigate the effect of metal ions on chromogenic and electrochemical sensing. To the best of our knowledge, dipyrrinato complexes containing both fcdpm and dithiocarbamates have not been synthesized and used as a multichannel sensor for Hg^{2+} and Pb^{2+} ions. Through this contribution we present novel complexes containing both fcdpm and dithiocarbamates and their application as chromogenic and redox sensors for Hg^{2+} and Pb^{2+} ions.

EXPERIMENTAL SECTION

Reagents. All synthetic manipulations were performed in deaerated solvents under a nitrogen atmosphere. Solvents were rigorously purified following literature procedures prior to use.[21] Diethyl/diisopropyl/dibutylamine, carbon disulfide, 2,3-dichloro-5,6-dicyano-1,4-benzoquinone (DDQ), 5-ferrocenylcarbaldehyde, pyrrole, tetrabutylammonium perchlorate $[(n\text{-}Bu)_4N]ClO_4$, and Ni(II) and Pd(II) chloride hydrate were used as received without further purification. Precursor complexes $[M(dtc)_2]$ (M = Ni, Pd; dtc = dedtc, dipdtc, dbdtc) and 5-ferrocenyldipyrromethene (fcdpm) were prepared and purified by literature procedures.[22]

General Methods. Elemental analyses for carbon, hydrogen, and nitrogen (C, H, and N) were performed on an Exeter Analytical Inc. model CE-440 CHN analyzer. IR and electronic absorption spectra were acquired on Varian 3300 FT-IR and Shimadzu UV-1601 and Cary 100 BIO UV−visible spectrophotometers, respectively. ^1H (300 MHz) and ^{13}C (75.45 MHz) NMR spectra were obtained on a JEOL AL300 FT-NMR spectrometer using tetramethylsilane $[Si(CH_3)_4]$ as an internal reference. Electrospray ionization mass spectrometric (ESI-MS) measurements were made on a THERMO Finningan LCQ Advantage Max ion trap mass spectrometer. Samples (10 μL) were dissolved in dichloromethane/acetonitrile (3:7, v/v) and introduced into the ESI source through a Finningan surveyor auto sampler. Mobile phase (MeOH/MeCN:H_2O, 90:10) flowed at a rate of 250 μL/min. The ion spray voltage was set at 5.3 KV, and the capillary voltage was set at 34 V. The MS scan run up to 2.5 min and spectra print outs were averaged of over 10 scans. Electrochemical measurements were performed on a CHI 620c electrochemical analyzer. All measurements were performed under a nitrogen atmosphere in a single-compartment cell equipped with a glassy carbon working electrode, platinum wire counter electrode, and Ag/Ag^{+} reference electrode.

Synthesis of [Ni(fcdpm)(dedtc)] (1). DDQ (0.227 g, 1.0 m mol) dissolved in benzene (30 mL) was added dropwise to an ice-cooled stirring solution of fcdpm (0.326 g, 1.0 m mol) in dichloromethane (40 mL), and the reaction mixture was stirred at room temperature for an additional 1 h. It was concentrated to dryness under reduced pressure to afford a dark red brown solid. The ensuing product was dissolved in dichloromethane (40 mL) and filtered to remove any solid impurities. Triethylamine (1 mL) and $[Ni(dedtc)_2]$ (0.182 g, 0.50 m mol) were successively added to the filtrate, and the reaction mixture was stirred overnight under a nitrogen atmosphere. It was concentrated to dryness, and the resulting product was purified by column chromatography (SiO_2; CH_2Cl_2/hexane, 60:40) to afford a dark red solid. Yield: 0.346 g; 65%. Anal. Calcd for $C_{24}H_{25}FeN_3NiS_2$: C, 53.97; H, 4.72; N 7.87. Found: C, 53.92; H, 4.68; N, 7.78. ^1H NMR ($CDCl_3$, δ_H ppm): 7.62 (d, 4H, J = 39 Hz), 6.99 (s, 2H), 6.27 (d, 2H, J = 36 Hz), 4.76 (s, 2H), 4.46 (s, 3H), 4.19 (s, 5H), 3.66 (q, 4H), 1.27 (t, 6H). ^{13}C NMR ($CDCl_3$, δ_C ppm): 202.35, 148.34, 147.79, 135.82, 131.21, 116.53, 83.49, 70.93, 68.98, 44.31, 12.36. ESI-MS calcd, found: m/z 535.0193, 535.0215 $[M]^+$. IR (KBr pellets, cm^{-1}): 486, 595, 668, 732, 772, 828, 887, 989, 1037, 1171, 1208, 1236, 1331, 1374, 1401, 1507, 1532, 1588, 1630, 2927. UV−vis (c = 100 μM; H_2O:EtOH, 50:50, v:v; pH ≈ 7.2; λ_{max} nm, ε M^{-1} cm^{-1}): 540 (1.38×10^4), 478 (2.36×10^4), 352 (1.80×10^4), 275 (2.54×10^4).

Synthesis of [Ni(fcdpm)(dipdtc)] (2). **2** was prepared following the above procedure for **1** using $[Ni(dipdtc)_2]$ in place of $[Ni(dedtc)_2]$. After routine work up and purification by column chromatography (SiO_2; CH_2Cl_2/hexane 50:50) **2** separated as a red crystalline compound. Yield: 0.325 g; 58%. Anal. Calcd for $C_{26}H_{29}FeN_3NiS_2$: C, 55.55; H, 5.20; N 7.47. Found: C, 55.48; H, 5.12; N 7.36. ^1H NMR ($CDCl_3$, δ_H ppm): 7.62 (d, 4H, J = 39 Hz), 6.99 (s, 2H), 6.27 (d, 2H, J = 36 Hz), 4.76 (s, 2H), 4.46 (s, 3H), 4.19 (s, 5H), 3.66 (m, 6H), 1.57 (m, 6H), 1.45 (m, 6H), 1.29 (m, 2H). ^{13}C NMR ($CDCl_3$, δ_C ppm): 201.32, 147.95, 147.71, 135.93, 131.15, 116.46, 83.55, 74.51, 70.91, 68.94, 51.31, 19.46. ESI-MS calcd, found:

dx.doi.org/10.1021/ic300900m | Inorg. Chem. 2012, 51, 8916−8930

m/*z* 561.0506, 561.0547 $[M]^+$. IR (KBr pellets, cm^{-1}): 656, 719, 739, 770, 776, 889, 995, 1032, 1207, 1247, 1346, 1380, 1410, 1510, 1536, 1595, 1561, 1637, 3028, 3100. UV−vis (c = 100 μM; H_2O:EtOH, 50:50, v:v; pH ≈ 7.2; λ_{max} nm, ε M^{-1} cm^{-1}): 530 (0.84×10^4), 480 (1.21×10^4), 339 (1.23×10^4).

Synthesis of [Ni(fcdpm)(dbdtc)] (3). **3** was prepared following the above procedure for **1** except that $[Ni(dbdtc)_2]$ was used in place of $[Ni(dedtc)_2]$. After purification by column chromatography (SiO_2; CH_2Cl_2:Hexane; 50:50) it was isolated as a red crystalline compound. Yield: 0.374 g 59%. Anal. Calcd for $C_{28}H_{33}FeN_3NiS_2$: C, 56.98; H, 5.64; N, 7.12. Found: C, 56.88; H, 5.60; N, 7.03. ^1H NMR ($CDCl_3$, δ_H ppm): 7.62 (d, 4H, J = 39 Hz), 6.99 (s, 2H), 6.27 (d, 2H, J = 36 Hz), 4.76 (s, 2H), 4.46 (s, 3H), 4.19 (s, 5H), 3.55 (m, 4H), 1.56 (m, 4H), 1.34 (m, 4H), 0.954 (m, 6H). ^{13}C NMR ($CDCl_3$, δ_C ppm): 202.86, 148.33, 147.95 135.85, 131.20, 116.54, 83.52, 74.52, 70.93, 68.96, 49.56, 30.25, 26.87, 19.98, 13.68. ESI-MS calcd, found: *m*/*z* 589.0819, 590.0918 $[M + 1]^+$. IR (KBr pellets, cm^{-1}): 657, 718, 735, 771, 773, 892, 994, 1030, 1208, 1245, 1346, 1385, 1411, 1509, 1537, 1596, 1563, 1634, 3029, 3112. UV−vis (c = 100 μM; H_2O:EtOH, 50:50, v/v; pH ≈ 7.2; λ_{max} nm, ε M^{-1} cm^{-1}): 532 (0.84×10^4), 475 (2.36×10^4), 393 (1.01×10^4), 323 (5.36×10^4).

Synthesis of [Pd(fcdpm)(dedtc)] (4). **4** was prepared by the above procedure for **1** except $[Pd(dedtc)_2]$ (0.196 g, 0.25 m mol) was used in place of $[Ni(dedtc)_2]$. After routine workup it gave a red brown solid, which upon purification by column chromatography (SiO_2; CH_2Cl_2/hexane, 50:50) afforded the desired product (dark red solid). Yield: 0.102 g; 52%. Anal. Calcd for $C_{24}H_{25}FeN_3PdS_2$: C, 49.54; H, 4.33; N 7.22. Found: C, 49.39; H, 4.68; N, 7.38. ^1H NMR ($CDCl_3$, δ_H ppm): 7.74 (d, 2H, J = 3.6 Hz), 7.28 (s, 2H), 6.38 (d, 2H, J = 3.6 Hz), 4.80 (s, 2H), 4.48 (s, 2H), 4.17 (s, 5H), 3.78 (q, 4H), 1.34 (t, 6H). ^{13}C NMR ($CDCl_3$, δ_C ppm): 206.91, 149.83, 147.79, 134.96, 130.51, 116.04, 84.48, 75.04, 70.97, 68.81, 44.52, 12.43. ESI-MS calcd, found: *m*/*z* 580.9874, 581.0026 $[M]^+$. IR (KBr pellets, cm^{-1}): 476, 725, 767, 805, 829, 994, 1035, 1208, 1243, 1280, 1337, 1376, 1404, 1437, 1519, 3441. UV−vis (c = 10 μM; H_2O:MeCN, 10:90, v:v; pH ≈ 7.6; λ_{max} nm, ε M^{-1} cm^{-1}): 598 (5.4×10^3), 509 (6.15×10^4), 414 (1.45×10^4), 343 (2.94×10^4), 298, (3.50×10^4).

Synthesis of [Pd(fcdpm)(dipdtc)] (5). Complex **5** was prepared following the above procedure for **1** using $[Pd(dipdtc)_2]$ in place of $[Ni(dedtc)_2]$. After purification by column chromatography (SiO_2; CH_2Cl_2:hexane; 50:50) it was isolated as blue green crystals. Yield: 0.325 g; 58%. Anal. Calcd for $C_{26}H_{29}FeN_3PdS_2$: C, 51.20; H, 4.79; N 6.89. Found: C, 51.38; H, 4.68; N 6.75. ^1H NMR ($CDCl_3$, δ_H ppm): 7.62 (d, 4H, J = 39 Hz), 6.99 (s, 2H), 6.27 (d, 2H, J = 36 Hz), 4.76 (s, 2H), 4.46 (s, 3H), 4.19 (s, 5H), 3.66 (m, 6H), 1.57 (m, 6H), 1.45 (m, 6H), 1.29 (m, 2H). ^{13}C NMR ($CDCl_3$, δ_C ppm): 205.90, 149.87, 147.78, 134.41, 130.51, 116.04, 84.53, 75.04, 70.83, 68.29, 54.53, 16.03. ESI-MS calcd, found: *m*/*z* 609.0187, 609.0313 $[M]^+$. IR (KBr pellets, cm^{-1}): 581, 722, 764, 800, 830, 887, 993, 993, 1034, 1142, 1191, 1333, 1374, 1495, 1448, 1521, 3443. UV−vis (c = 10 μM; H_2O:MeCN, 10:90, v:v; pH ≈ 7.6; λ_{max} nm, ε M^{-1} cm^{-1}): 598 (5.3×10^3), 509 (6.10×10^4), 414 (1.41×10^4), 343 (2.92×10^4), 298, (2.58×10^4).

Synthesis of [Pd(fcdpm)(dbdtc)] (6). **6** was prepared following the above procedure for **1** using $[Pd(dbdtc)_2]$ in place of $[Ni(dedtc)_2]$. After purification by column chromatography (SiO_2; CH_2Cl_2:hexane; 50:50) it was isolated as blue green crystals. Yield: 0.374 g 59%. Anal. Calcd for $C_{28}H_{33}FeN_3PdS_2$: C, 52.55; H, 5.51; N, 6.57. Found: C, 52.84; H, 5.60; N, 6.43. ^1H NMR ($CDCl_3$, δ_H ppm): 7.74 (d, 2H, J = 3.6 Hz), 7.29 (s, 2H), 6.37 (d, 2H, J = 3.0 Hz), 4.80 (s, 2H), 4.48 (s, 2H), 4.17 (s, 5H), 3.70 (t, 4H), 1.71 (m, 4H), 1.43 (m, 4H), 0.98 (m, 6H). ^{13}C NMR ($CDCl_3$, δ_C ppm): 205.88, 152.36, 130.51, 127.07, 116.97, 85.10, 112.79, 107.75, 87.98, 86.29, 85.53, 82.95, 81.15, 72.72, 70.98, 47.91, 39.36, 37.56, 35.90, 33.51, 20.08, 10.37, 6.10. ESI-MS. calcd, found: *m*/*z* 637.0500, 637.0654 $[M]^+$. IR (KBr pellets, cm^{-1}): 501, 601, 729, 769, 805, 829, 995, 1037, 1108, 1245, 1335, 1374, 1431, 1520, 3421. UV−vis (c = 10 μM; H_2O:MeCN, 10:90, v/v; pH ≈ 7.6; λ_{max} nm, ε M^{-1} cm^{-1}): 509 (1.06×10^4), 414 (0.18×10^4), 343 (1.42×10^4), 298, (10.24×10^4).

Synthesis of $[2{\cdot}Hg(H_2O)_2(NO_3)]^+$ (7). A solution of **2** (0.280 g, 0.5 mmol) in EtOH (20 mL) was treated with $Hg(NO_3)_2{\cdot}H_2O$ (0.80 g, 2.5 mmol) dissolved in water (5.0 mL), and the reaction mixture was stirred at room temperature for 2 h, whereupon the brown color of the solution turned yellowish green. After stirring for an additional 7−8 h, it was concentrated to dryness and the resulting product dried under vacuum. Product yield and elemental analyses for **7** could not be estimated due to the presence of an excess of $Hg(NO_3)_2{\cdot}H_2O$. ESI-MS calcd, found: *m*/*z* 761.6406, 762.1655 $[2 + Hg + 1]^+$, 856.5658, 857.2476 $[2 + Hg + 2H_2O + NO_3^- + 1]^+$. IR (KBr pellets, cm^{-1}): 657, 724, 772, 776, 890, 1005, 1033, 1206, 1243, 1345, 1384, 1410, 1497, 1510, 1536, 1595, 1561, 1637, 3435. UV−vis (c = 100 μM; H_2O:EtOH, 50:50, v:v; pH ≈ 7.2; λ_{max} nm, ε M^{-1} cm^{-1}): 710 (0.33×10^4), 480 (1.94×10^4), 393 (1.04×10^4).

Synthesis of $[2{\cdot}Pb(H_2O)_2(NO_3)]^+$ (8). **8** was prepared following the above procedure for **7** using $Pb(NO_3)_2$ (0.827 g, 2.5 mmol). ESI-MS calcd, found: *m*/*z* 866.0367, 866.0954 $[2 + Pb + 2H_2O + NO^{3-}]^+$. IR (KBr pellets, cm^{-1}): 654, 725, 775, 890, 1007, 1035, 1238, 1345, 1384, 1409, 1500, 1511, 1536, 1599, 1637, 3436. UV−vis (c = 100 μM; H_2O:EtOH, 50:50, v:v; pH ≈ 7.2; λ_{max} nm, ε M^{-1} cm^{-1}): 701 (0.37×10^4), 530 (0.36×10^4) 480 (1.45×10^4), 393 (0.81×10^4).

Synthesis of $[4{\cdot}Hg(H_2O)_2(NO_3)]^+$ (9). **9** was prepared following the above procedure for **7** using **4** (0.290 g, 0.5 mmol; MeCN) in place of **2**. ESI-MS calcd, found: *m*/*z* 881.0108, 881.2868 $[4 + Hg + 2H_2O + NO^{3-}]^+$. IR (KBr pellets, cm^{-1}): 637, 726, 774, 775, 896, 1010, 1036, 1208, 1245, 1348, 1390, 1414, 1494, 1514, 1538, 1598, 1639, 3439. UV−vis (c = 10 μM; H_2O:MeCN, 10:90, v:v; pH ≈ 7.6; λ_{max} nm, ε M^{-1} cm^{-1}): 710 (0.71×10^4), 477 (7.94×10^4), 394 (3.56×10^4).

X-ray Structure Determination. Crystals suitable for single-crystal X-ray diffraction analyses for **1**, **2**, **4**, and **5** were obtained by slow diffusion of hexane over a dichloromethane solution of the respective complexes. X-ray data on **1**, **2**, and **4** were collected on a R-AXIS RAPID II and **5** on Bruker APEX II (kappa 4) diffractometer at room temperature with Mo Kα radiation (λ = 0.71073 Å) at the single-crystal X-diffraction centers of the National Institute of Advanced Industrial Science and Technology (AIST), Osaka, Japan and the National Institute of Science Education and Research (NISER) Bhubaneshwar, India. Structures were solved by direct methods (SHELXS 97) and refined by full-matrix least-squares calculations on F^2 (SHELX 97).[23] All non-H atoms were treated anisotropically. H atoms attached to carbon were included as a fixed contribution and geometrically calculated and refined using the SHELX riding model. The computer program PLATON was used for analyzing the interaction and stacking distances.[24] CCDC deposition Nos. 856055 (**1**), 856056 (**2**), 868304 (**4**), and 868305 (**5**) contain supplementary crystallographic data for this paper. Data can be obtained free of charge via http://www.ccdc.cam.ac.uk/conts/retrieving.html (or from the CCDC, 12 Union Road, Cambridge CB2 1EZ, U.K. Fax: +44-1223-336033. E-mail: deposit@ccdc.cam.ac.uk).

Electrochemical Measurements. The redox behavior of **1**−**6** has been investigated by cyclic and differential pulse voltammetry (MeCN, 100 μM) in the potential range from +2.0 to −2.0 V at a scan rate of 100 mV s^{-1}. Measurements were performed at room temperature using tetrabutylammonium perchlorate $[(n\text{-}Bu)_4N]ClO_4$ (0.1 M) as a supporting electrolyte, and redox potentials were referenced to the Fc/Fc^+ couple (0.1 V). The metal ion effect and titration studies have been performed using 3.0 mL of a solution of **1**−**6** and 0.1 M nitrate salt of various metal ions (Na^+, K^+, Mg^{2+}, Ca^{2+}, Fe^{3+}, Co^{2+}, Ni^{2+}, Cu^{2+}, Zn^{2+}, Cd^{2+}, Hg^{2+}, Ag^+, and Pb^{2+}).

UV−Vis Studies. Stock solutions (c = 10 μM) for electronic absorption studies were prepared in water−ethanol (50:50; v:v; **1**−**3**) and water−acetonitrile (10:90, v:v; **4**−**6**), while solutions of the tested metal ions viz. Na^+, K^+, Ca^{2+}, Mg^{2+}, Mn^{2+}, Fe^{2+}, Co^{2+}, Ni^{2+}, Cu^{2+}, Zn^{2+}, Ag^+, Cd^{2+}, Hg^{2+}, and Pb^{2+} were prepared by dissolving their nitrate salts in triple-distilled water (c = 10 mM). In a typical titration study 3.0 mL of a solution of the complexes (c = 10 μM) was taken in a quartz cell (path length, 1 cm), and a solution of the metal ions (c = 10 mM) was added gradually with the help of a micropipette. In these

dx.doi.org/10.1021/ic300900m | *Inorg. Chem.* 2012, 51, 8916−8930

Scheme 1. Preparation of 5-Ferrocenyldipyrromethene and Heteroleptic Complexes 1−6

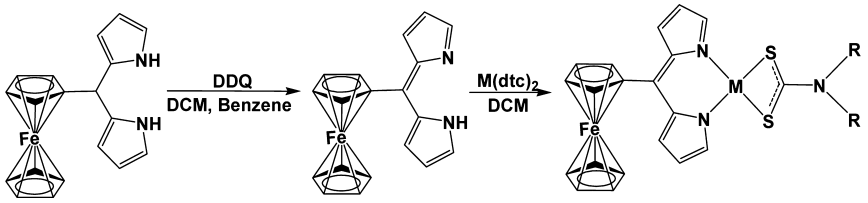

Table 1. Crystal Data and Structure Refinement Parameters for 1, 2, 4, and 5

	1	2	4	5
empirical formula	$C_{24}H_{25}FeN_3NiS_2$	$C_{26}H_{29}FeN_3NiS_2$	$C_{24}H_{25}FeN_3PdS_2$	$C_{26}H_{29}FeN_3PdS_2$
cryst syst	orthorhombic	tetragonal	monoclinic	tetragonal
space group	*Pbca*	$P4_1$	$P2_1/c$	$P4_1$
a (Å)	14.722(3)	15.394(2)	13.696(3)	15.439(10)
b (Å)	13.733(3)	15.394(2)	14.344(3)	15.439(10)
c (Å)	25.207(5)	12.146(2)	13.845(3)	12.184(2)
α (deg)	90.00	90.00	90.00	90.00
β (deg)	90.00	90.00	95.75(3)	90.00
γ (deg)	90.00	90.00	90.00	90.00
V (Å^3), *Z*	5096.2(17), 8	2878.2(8), 4	2706.3(9), 4	2904.32(5), 4
λ (Å)	0.71073	0.71073	0.71073	0.71073
color and habit	red, block	red, needle	red, block	red, needle
T (K)	293(2)	293(2)	293(2)	293(2)
reflns collected	3145	5233	2947	4664
refins/restraint/params	4464/0/282	6436/0/302	4710/29/357	5104/1/302
D_{calcd} (Mg m^{-3})	1.392	1.297	1.428	1.395
μ (mm^{-1})	1.487	1.320	1.369	1.279
GOF on F^2	1.069	1.076	1.028	1.158
final *R* indices $I > 2\sigma(I)$	R1 = 0.0541	R1 = 0.0399	R1 = 0.0615	R1 = 0.0287
	wR2 = 0.1391	wR2 = 0.0985	wR2 = 0.1503	wR2 = 0.0811
R indices (all data)	R1 = 0.0793	R1 = 0.0554	R1 = 0.1093	R1 = 0.0334
	wR2 = 0.1564	wR2 = 0.1072	wR2 = 0.1743	wR2 = 0.0844

experiments the addition interval time for each aliquot of the metal ion (Hg^{2+}/Pb^{2+}) was 30 s.

Quantum Chemical Calculation. Quantum chemical calculations have been performed to understand the binding sites and also verify the composition of the complexes. Our experience showed that the density functional theory (DFT) methods are most feasible for calculations.[25] In this context a hybrid version of DFT and Hartree−Fock (HF) methods was used, namely, the B3LYP density functional theory method in which the exchange energy from Becke's exchange functional is combined with exact energy from Hartree−Fock theory.[26a,b] Along with component exchange and correlation functionals three parameters define the hybrid functional specifying how much of the exact exchange is mixed in. Basis set 6-31G** has been used for all atoms other than Hg or Pb, while LANL2DZ was used with an effective core pseudo potential for these metals.[26c,d] Geometry optimization and frequency calculations (to verify a genuine minimum energy structure) have been performed using the Gaussian 03 suite of programs.[26e] The nitrate anion occupying one of the coordination sites was reoptimized using the 6-31+G** basis set (with no change in basis set for metal atoms) starting at the optimized geometry using the 6-31G** basis set to account for the contribution of the tail part of atomic bases. Our calculations reveal that there is no significant change in geometry.

RESULTS AND DISCUSSION

Synthesis and Characterization. The precursor complexes [M(dtc)$_2$] (M = Ni, Pd; dtc = dedtc, dipdtc, dbdtc) reacted with fcdpm obtained by in situ oxidation of 5-ferrocenyldipyrromethane with 2,3-dichloro-5,6-dicyano-1,4-benzoquinone (DDQ) in CH_2Cl_2/C_6H_6 at room temperature to afford heteroleptic dipyrrinato complexes [Ni(fcdpm)(dedtc)] (**1**), [Ni(fcdpm)(dipdtc)] (**2**), [Ni(fcdpm)(dbdtc)] (**3**), [Pd(fcdpm)(dedtc)] (**4**), [Pd(fcdpm)(dipdtc)] (**5**), and [Pd(fcdpm)(dbdtc)] (**6**). The simple synthetic strategy adopted for preparation of fcdpm and complexes **1**−**6** is depicted in Scheme 1. These were obtained in moderate yields (∼50−65%) after extractive workup, purification by column chromatography, and crystallization from dichloromethane/hexane. The complexes under investigation are nonhygroscopic, air-stable crystalline solids, highly soluble in common organic solvents like dichloromethane, chloroform, acetone, dimethylsulfoxide, and acetonitrile, and sparingly soluble in methanol, ethanol, diethyl ether, petroleum ether, and hexane. All complexes have been characterized by satisfactory elemental analyses, spectral (ESI-MS, IR, ^{1}H, ^{13}C NMR, UV−vis), and electrochemical studies. Crystal structures of **1**, **2**, **4**, and **5** have been authenticated by X-ray single-crystal analyses.

Spectral Studies. Infrared spectra of the complexes displayed diagnostic bands due to coordinated fcdpm and dtc. In general, IR spectra of dtc complexes exhibit bands due to νC=N (S_2−C=NR_2) and νC−S stretching vibrations at ∼1540 and 1034 cm^{-1}. The bands associated with νC=N (S_2−C=NR_2) in complexes **1**−**6** exhibited a shift of ∼5−10 cm^{-1} relative to the respective precursors [1537, Ni(dedtc)$_2$; 1540, Ni(dipdtc)$_2$; 1538, Ni(dbdtc)$_2$; 1545, Pd(dedtc)$_2$; 1548, Pd(dipdtc)$_2$; 1546, Pd(dbdtc)$_2$] and vibrated at ∼1532 (**1**), 1536 (**2**), 1533 (**3**), 1534 (**4**), 1543 (**5**), and 1542 cm^{-1} (**6**). In addition, νC−S stretching vibrations occurred at ∼1034 cm^{-1}

dx.doi.org/10.1021/ic300900m | Inorg. Chem. 2012, 51, 8916−8930

Table 2. Selected Bond Lengths (Angstroms) and Angles (degrees) for 1, 2, 4, and 5

	1	2		4	5
Ni−N1	1.89(4)	1.90(3)	Pd−N1	2.01(11)	2.028(3)
Ni−N2	1.89(3)	1.89(3)	Pd−N2	2.01(11)	2.026(4)
Ni−S1	2.20(16)	2.20(10)	Pd−S1	2.311(5)	2.2900(11)
Ni−S2	2.21(16)	2.20(11)	Pd−S2	2.356(13)	2.2922(11)
Fe−η^5-Cp1	1.65	1.66	Fe−η^5-Cp1	1.66	1.66
Fe−η^5-Cp2	1.65	1.67	Fe−η^5-Cp2	1.67	1.67
C20−S1	1.70(6)	1.72(4)	C20−S1	1.72(18)	1.723(5)
C20−S2	1.71(6)	1.71(4)	C20−S2	1.73(2)	1.723(4)
C20−N3	1.33(7)	1.32(5)	C20−N3	1.33(19)	1.310(5)
N2−Ni−N1	92.58(15)	92.07(12)	N2−Pd−N1	88.9(2)	88.70(13)
N2−Ni−S1	172.80(12)	171.81(10)	N2−Pd−S1	96.2(2)	171.79(10)
N1−Ni−S1	94.61(11)	95.22(9)	N1−Pd−S1	170.3(2)	98.60(9)
N2−Ni−S2	95.00(12)	95.14(10)	N2−Pd−S2	170.6(4)	97.56(10)
N1−Ni−S2	172.04(11)	172.79(9)	N1−Pd−S2	98.2(4)	173.64(9)
S1−Ni−S2	77.83(6)	77.56(4)	S1−Pd−S2	75.9(4)	75.08(4)
N3−C20−S1	125.5(5)	127.5(3)	N3−C20−S1	123.7(14)	126.3(3)
N3−C20−S2	125.5(5)	126.0(3)	N3−C20−S2	122.9(15)	125.4(3)
S1−C20−S2	109.0(3)	106.44(19)	S1−C20−S2	112.6(9)	108.2(2)
C20−S2−Ni	86.2(2)	87.97(13)	C20−S2−Pd	84.8(8)	88.21(15)
C20−S1−Ni	86.9(2)	87.98(13)	C20−S1−Pd	86.5(6)	88.31(15)
ω	2.58	3.78	ω	9.28	13.23

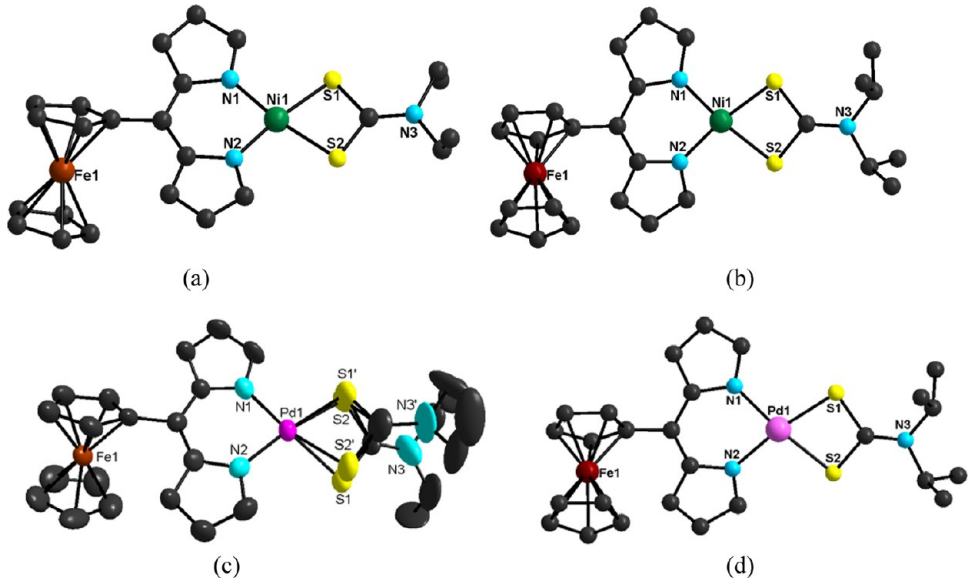

Figure 1. Crystal structures of **1** (a), **2** (b), **4** (c), and **5** (d). Hydrogen atoms have been omitted for clarity. dedtc moiety in **4** is disordered, showing equal probability to lie above and below the plane.

without any splitting. The appearance of unsplit bands due to νC=N and νC−S supported the bidentate coordination of dtc.[27] νC=N of coordinated fcdpm vibrated as split bands at 1507 (**1**), 1510 (**2**), 1509 (**3**), 1519 (**4**), 1521 (**5**), and 1520 (**6**) cm^{-1}.[20d,28]

^{1}H NMR spectral data of the complexes corroborated well with their proposed formulations. Notably, the protons associated with ligands and precursor complexes resonated at almost the same position. Protons corresponding to fcdpm in nickel complexes **1**−**3** resonated at ∼4.19 (*Cp*), 4.46 (*Cp*), 4.76 (*Cp*), 6.27 (pyrrole), 6.99 (pyrrole), and 7.62 ppm (pyrrole), while those in palladium complexes **4**−**6** resonated at ∼4.17 (*Cp*), 4.47 (*Cp*), 4.80 (*Cp*), 6.37 (pyrrole), 7.28 (pyrrole), and 7.74 ppm (pyrrole). The α and β protons [N-$(CH_2)_2(CH_3)_2$; N-$(CH_2)_2(CH_3)_2$] of dedtc in **1** and **4** displayed a downfield shift of ∼0.05 ppm [∼3.66, 1.27 ppm, **1**; 3.77, 1.34 ppm, **4**]. Deshielding of these protons may be ascribed to complexation of the ligand with the metal center. Similarly, α and β protons of dipdtc in **2** and **5** resonated at their usual position [∼3.66, 1.27 ppm, **2**; 1.56 and 1.51 ppm, **5**]. The α, β, γ, and δ protons of **3** and **6** resonated at ∼3.56, 1.64, 1.38, and 0.96 ppm, respectively (Figures S1a−S6a, Supporting Information).[20d,27,28] Markedly, the protons corresponding to **2** and **3** exhibited negligible shift relative to their precursor complexes like those of **1** and **4**. ^{13}C NMR spectra of **1**−**6** displayed an analogous pattern of resonances and supported proposed formulations. Resulting data are summarized in the Experimental Section and spectra shown in Figures S1b−S6b, Supporting Information. Low-intensity resonances due to the S_2−C=NR_2 carbon of these complexes were displayed at 202.36

dx.doi.org/10.1021/ic300900m | *Inorg. Chem.* 2012, 51, 8916−8930

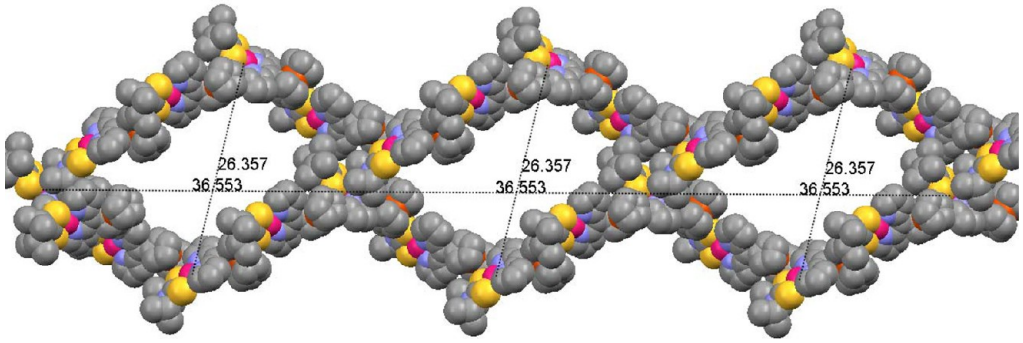

Figure 2. Double-helical motif in **4** along the crystallographic '*b*' axis arising from C−H···S interactions.

(**1**), 201.33 (**2**), 202.86 (**3**) 206.91 (**4**), 205.90 (**5**), and 205.88 ppm (**6**).[27]

Crystal Structures. The molecular structures of **1**, **2**, **4**, and **5** have been authenticated crystallographically. Detailed crystallographic data and selected geometrical parameters are summarized in Tables 1 and 2 and structures depicted in Figure 1a−d. Complex **1** crystallizes in the orthorhombic system with the *Pbca* space group, while **2** in is in a tetragonal system with the $P4_1$ space group. The immediate coordination geometry in both **1** and **2** is distorted square planar defined by S1 and S2 from dtc and N1 and N2 from fcdpm. The observed distortion from square planar geometry about the metal center may be attributed to small bite angles (N1−Ni−N2, 92.58° and S1−Ni−S2, 77.83°, **1**; N1−Ni−N2, 92.07° and S1−Ni−S2, 77.56°; **2**). The Ni−N [Ni−N1, 1.89 Å; Ni−N2, 1.89 Å] and Ni−S bond distances [Ni−S1, 2.20 Å; Ni−S2, 2.21 Å] and various bond angles [N1−Ni−N2 92.58°; S1−Ni−S2, 77.83°; N1−Ni−S1, 94.61°; N2−Ni−S2, 95.00°] in **1** are normal and comparable to other related systems.[20d,29,30] The decrease in the C20−N3 bond distance (1.33 Å) and increase in the S−C−N angle (S1−C20−N3, 125.5°; S2−C20−N3, 125.4°) result from delocalization of π electron density over the S2CN moiety. In the same way, Ni−N and Ni−S bond distances [Ni−N1, 1.90 Å; Ni−N2, 1.89 Å; Ni−S1, 2.20 Å; Ni−S2, 2.20 Å] and bond angles [N1−Ni−N2, 92.07°; S1−Ni−S2, 77.56°; N1−Ni−S1, 95.22°; N2−Ni−S2, 95.14°] in **2** are comparable to those in **1** and in accordance with earlier reports.[20d,29,30] The C20−N3 [S2−C$^{\cdots}$NR$_2$] bond distance (1.32 Å) and S−C−N bond angles (S1−C20−N3, 127.5°; S2−C20−N3, 126.0°) are also comparable to **1**. The cyclopentadienyl rings of the ferrocenyl moieties are almost planar and inclined from the dipyrrin plane by 41.29° (**1**) and 48.15° (**2**).

Complex **4** crystallizes in the monoclinic system with the $P2_1/c$ space group and **5** in a tetragonal system with the $P4_1$ space group. The immediate coordination geometry about the palladium center in these complexes is distorted square planar and defined by N1, N2 from fcdpm and S1, S2 from dtc. The observed distortion from square planar geometry about the palladium center arises from twisted angles between dtc and fcdpm planes [9.28°, **4**; 13.23°, **5**]. Pd−N and Pd−S bond distances [Pd−N1, 2.01 Å; Pd−N2, 2.01 Å; Pd−S1, 2.31 Å; Pd−S2, 2.34 Å] and various bond angles [N1−Pd−N2, 88.9°; S1−Pd−S2, 170.3°; N1−Pd−S1, 170.3°; N2−Pd−S2, 170.6°] in **4** are normal and comparable to those in other related systems.[14d,31] It is worth mentioning that the dedtc moiety in **4** shows disorder wherein entire dtc unit has equal possibility to lie above and below the plane. The Pd−S bond distances are almost equal in both disordered units. Delocalization of the π electron density over the S2CN moiety leads to a decrease in the C20−N3 bond distance (1.33 Å) and an increase in the S−C−N angles [S1−C20−N3, 123.7°; S2−C20−N3, 122.9°]. The C20−N3 bond distance is intermediate between C−N (1.47 Å) and C═N (1.28 Å) and shows partial double-bond character. Similarly, Pd−N and Pd−S bond distances [Pd−N1, 2.02 Å; Pd−N2, 2.02 Å; Pd−S1, 2.29 Å; Pd−S2, 2.29 Å] and angles [N1−Pd−N2, 88.70°; S1−Pd−S2, 75.08°; N1−Pd−S1, 98.6°; N2−Pd−S2, 96.3°] in **5** are comparable to earlier reports.[14d,31] The C20−N3 [S2−C$^{\cdots}$NR$_2$] bond distance (1.31 Å) and S−C−N bond angles (S1−C20−N3, 126.3°; S2−C20−N3, 125.4°) are comparable to **4**. The ferrocenyl unit is inclined with respect to the dipyrrin moiety by 41.44° (**4**) and 48.54° (**5**), and Fe−C bond distances are normal and comparable to other reports (1.63−1.67 Å).

Weak bonding studies on these complexes revealed the presence of various types of weak bonding interactions leading to interesting motifs. Complexes **1** and **4** displayed only C−H···S (range, 3.060−3.30 Å, **1**; 3.065−3.32 Å, **4**) and C−H···π (2.885 Å, **1**; 2.895 Å, **4**) interactions, leading to a bilayered structural motif (Figure S7a,b, Supporting Information). On the other hand, C−H···S (range, 3.06−3.30 Å, **2**; 3.065−3.32 Å, **5**) leads to a single-stranded helix in **2** and **5** with an edge-to-face interaction between the cyclopentadienyl ring hydrogen and the sulfur from the adjacent molecules. In the helical structure of **2** each repeating unit consists of four molecules, and the distance between Ni and next repeating unit is 36.439 Å. Further, parallel extension leads to an antiparallel double-helical structure, wherein distance between the Ni center and the parallel unit is 26.421 Å (Figure S8, Supporting Information). Likewise, in the helical structure of **5** each repeating unit consists of four molecules and the distance between the Pd−Pd centers is 36.553 Å. Further, parallel extension leads to an antiparallel double-helical structure with Pd−Pd distances of 26.357 Å in the parallel units (Figure 2). Observed weak bonding interaction distances are in accordance with reported values.[32]

Visual Detection of Hg^{2+} and Pb^{2+}. The complexes under investigation are a colored solution, and in the presence of other metal ions these may exhibit a distinctive color change. This change in color may form the basis for naked eye visible detection. In a follow up of our studies solutions of **1**−**6** (100 μM) were treated with various metal ions viz., Na^+, K^+, Mg^{2+}, Ca^{2+}, Fe^{2+}, Co^{2+}, Ni^{2+}, Cu^{2+}, Zn^{2+}, Cd^{2+}, Pb^{2+}, Ag^+, and Hg^{2+} (10.0 equiv; c = 100 mM, nitrate salts). Notably, addition of only Hg^{2+}/Pb^{2+} (1.0 equiv) to a solution of **1**−**3** (c = 100 μM; H_2O:EtOH, 50:50, v/v, pH ≈ 7.2) displayed a distinctive color change (brown to yellowish green) and other metal ions were

dx.doi.org/10.1021/ic300900m | *Inorg. Chem.* 2012, 51, 8916−8930

ineffective in this regard (Figures 3 and 2; Figure S9, Supporting Information, **1** and **3**).

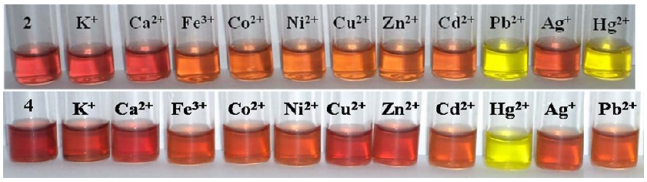

Figure 3. Changes in the color of solutions of **2** (c = 100 μM; H_2O:EtOH, 50:50, v/v; pH ≈ 7.2) and **4** (c = 100 μM; H_2O:MeCN, 10:90, v/v; pH ≈7.6) with 10.0 equiv of various metal ions (100 mM).

In the same way **4**–**6** (c = 100 μM; H_2O:MeCN, 10:90, v/v; pH ≈ 7.6) displayed a distinctive color change (Figures 3 and 4; Figure S9, Supporting Information, **5** and **6**) only in the

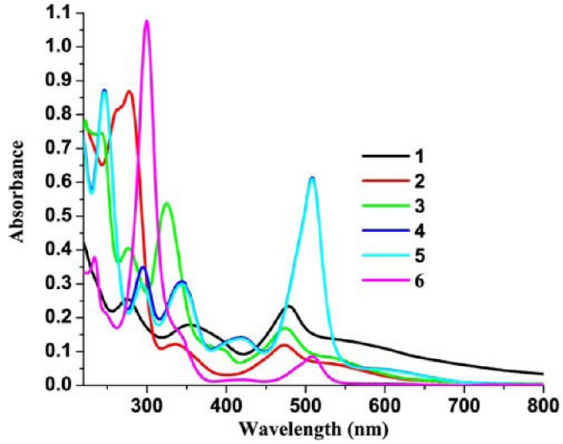

Figure 4. Absorption spectra of **1**–**3** (c = 10 μM; H_2O:EtOH, 50:50, v/v; pH ≈ 7.2) and **4**–**6** (c = 10 μM; H_2O:MeCN, 10:90, v/v; pH ≈ 7.6).

presence of Hg^{2+} (5.0 equiv). It clearly indicated the relatively high sensitivity of Ni–fcdpm complexes **1**–**3** for Hg^{2+}/Pb^{2+} and Pd–fcdpm complexes **4**–**6** for Hg^{2+}. Further, the colorimetric response toward Hg^{2+}/Pb^{2+} ions persisted for longer durations (>72 h), suggesting that **1**–**3** can act as a potential chromogenic sensor for Hg^{2+}/Pb^{2+} and **4**–**6** for Hg^{2+} ions.

UV–Vis Absorption Studies. Electronic absorption spectra of **1**–**6** are depicted in Figure 4, and resulting data are gathered in Table 3. UV–vis spectra of **1**–**3** (c = 100 μM; H_2O:EtOH, 50:50, v/v; pH ≈ 7.2) exhibited weak low-energy

Table 3. Electronic Absorption Spectral Data of 1–6

complexes	wavelength/nm (ε/M^{-1} cm^{-1})
1	540 (1.38×10^4), 478 (2.36×10^4), 352 (1.80×10^4), 275 (2.54×10^4)
2	530 (0.84×10^4), 480 (1.21×10^4), 339 (1.23×10^4)
3	532 (0.84×10^4), 475 (2.36×10^4), 393 (1.01×10^4), 323 (5.36×10^4)
4	598 (5.4×10^3), 509 (6.15×10^4), 414 (1.45×10^4), 343 (2.94×10^4), 298, (3.50×10^4)
5	598 (5.3×10^3), 509 (6.10×10^4), 414 (1.41×10^4), 343 (2.92×10^4), 298, (2.58×10^4)
6	509 (1.06×10^4), 414 (0.18×10^4), 343 (1.42×10^4), 298, (10.24×10^4)

(LE) absorptions at ~540–532 nm due to MLCT and strong transitions at ~478 nm attributable to π–π^* charge transfer processes associated with the dipyrrin moiety. In addition, these displayed intense bands in the UV region [352, 275 nm, **1**; 339 nm, **2**; 393, 323 nm, **3**] assignable to intraligand transitions.[14,20] Spectra of **4**–**6** were acquired in H_2O:MeCN (10:90, v/v; c = 10 μM; pH ~7.6) due to the poor solubility in EtOH/MeOH. Weak low-energy bands at ~598 nm have been assigned to MLCT transitions, while those at ~509 and ~414 nm have been assigned to π–π^* charge transfer processes related to the dipyrrin moiety. Intense bands at ~343 and 298 nm in the UV region have been assigned to intraligand transitions.[14,20]

Metal Ion Sensing Behavior. Metal ion interaction studies on **1**–**3** have been investigated by electronic absorption studies (c = 10 μM; H_2O:EtOH, 50:50, v/v; pH ≈ 7.2). Electronic spectra of **1**–**3** do not show any substantial change in the presence of 10.0 equiv of the tested metal ions (c = 10 mM) viz., Na^+, Ca^{2+}, Mg^{2+}, Fe^{2+}, Co^{2+}, Ni^{2+}, Cu^{2+}, Zn^{2+}, Cd^{2+} except for Hg^{2+} and Pb^{2+}. Upon addition of Hg^{2+} (10 equiv) to a solution of **2** the LE band centered at 530 nm vanished and the one at 480 nm displayed a hyperchromic shift (ε = 1.94×10^4 M^{-1} cm^{-1}). In addition, new bands emerged at 393 (1.04×10^4 M^{-1} cm^{-1}) and 706 nm (0.33×10^4 M^{-1} cm^{-1}) and the color of the solution turned yellowish green. Likewise, a concurrent decrease and increase in the optical density of the bands at 530 (0.36×10^4 M^{-1} cm^{-1}) and 480 nm (1.45×10^4 M^{-1} cm^{-1}) occurred upon addition of Pb^{2+} (10 equiv) to a solution of **2**. Moreover, new bands emerged at 393 (0.81×10^4, M^{-1} cm^{-1}) and 701 nm (0.37×10^4, M^{-1} cm^{-1}) with a distinctive color change (yellowish green) (Figure 5). Analogous trends have been observed for **1** and **3** (Figure S10a, Supporting Information, **1**; and Figure S10b, Supporting Information, **3**) also.

The cation recognition behavior of **4**–**6** has also been followed by electronic absorption spectral studies in H_2O:MeCN (10:90 v/v; c = 10 μM; pH ≈ 7.6). Spectral changes have been monitored by addition of 10.0 equiv of the tested metal ions (c = 10 mM) (Figure 5), and in this case significant spectral alterations were observed only in the presence of Hg^{2+}. The band centered at ~598 nm vanished, and those at 509 and 414 nm displayed a blue shift (from 509 to 477 nm; $\Delta\lambda$, 32 nm and from 414 to 394 nm; $\Delta\lambda$, 20 nm) upon addition of Hg^{2+} to a solution of **4**. Further, bands at 343 (3.19×10^4 M^{-1} cm^{-1}) and 293 nm (3.99×10^4 M^{-1} cm^{-1}) exhibited substantial hypochromic shifts (2.69×10^4 and 1.67×10^4 M^{-1} cm^{-1}) with emergence of new band in the NIR (near-infrared) region at 710 nm (0.71×10^4 M^{-1} cm^{-1}), and the color of the solution turned yellowish green. Complexes **5** and **6** also exhibited analogous behavior in the presence of the tested metal ions (Figure S17, Supporting Information).

Absorption titration studies have been performed to understand the binding affinity of the metal ions. Addition of Hg^{2+} (0.1 equiv) to a solution of **2** (c = 10 μM; H_2O:EtOH, 50:50, v/v; pH ≈ 7.2) leads to a hypochromic shift of the bands at 530 and 339 nm. Further, the band at 480 nm showed a hyperchromic shift, and a new weak band emerged at 393 nm. An increase in the concentration of Hg^{2+} (0.2 equiv) causes a significant decrease in the optical density of band at 530 nm (ε, 0.48×10^4 M^{-1} cm^{-1}), while it enhanced for the bands at 480 (1.40×10^4 M^{-1} cm^{-1}) and 393 nm (0.47×10^4 M^{-1} cm^{-1}). Further enhancement in the concentration of Hg^{2+} (0.3–1.0 equiv) leads to complete loss of the bands at 530 and 339 nm, and the optical density of those at 710, 480, and 393 nm was

dx.doi.org/10.1021/ic300900m | Inorg. Chem. 2012, 51, 8916–8930

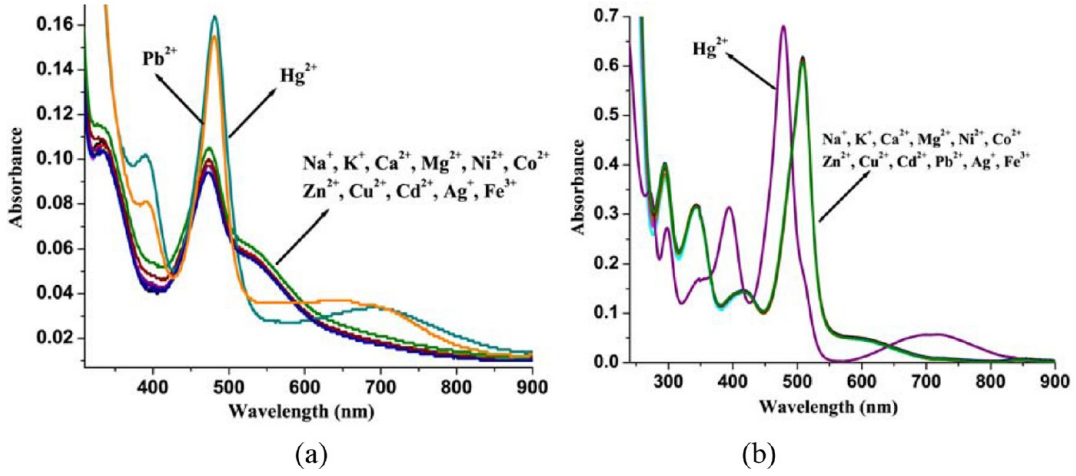

Figure 5. UV−vis spectra of **2** (c = 10 μM; H_2O:EtOH, 50:50, v/v; pH ≈ 7.2) (a) and **4** (c = 10 μM; H_2O:MeCN, 10:90 v/v; pH ≈ 7.6) (b) in the presence of various metal ions.

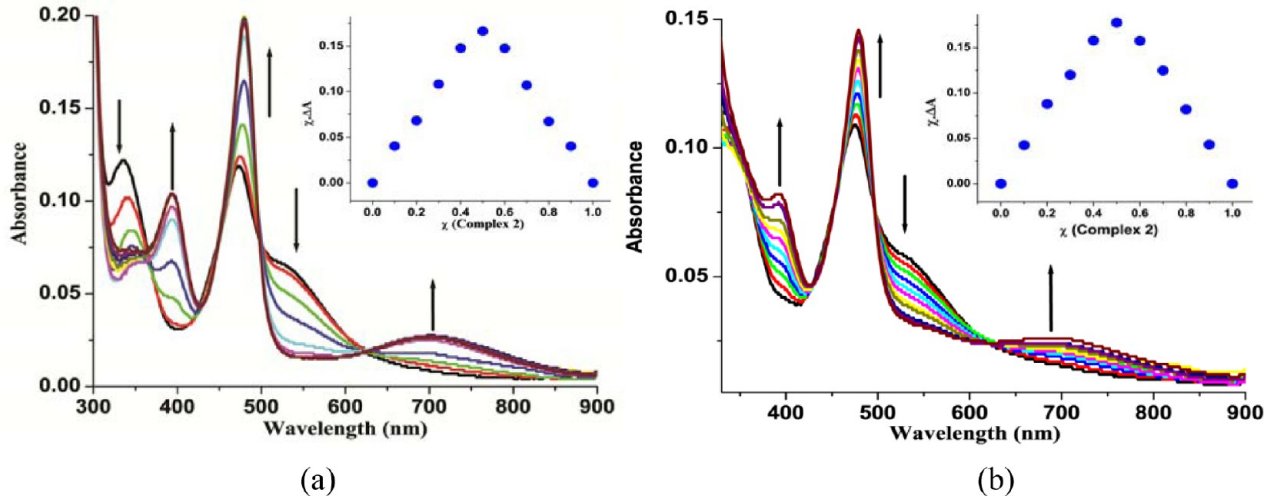

Figure 6. Evolution of the UV−vis spectrum of **2** (c = 10 μM; H_2O:EtOH, 50:50, v/v; pH ≈ 7.2) in the presence of various amounts of Hg^{2+} (a) and Pb^{2+} (b). (Insets) Job's plot for **2** with Hg^{2+} and Pb^{2+} indicating formation of 1:1.

significantly enhanced (0.33×10^4, 1.94×10^4, and 1.04×10^4 M^{-1} cm^{-1}). The presence of more than two species in the medium was indicated by isosbestic points at 624, 499, 448, and 426 nm in the titration curve. At saturation (1.0 equiv, Hg^{2+}) the titration curve exhibited three bands at 710, 480, and 393 nm, which have been ascribed to formation of **2**·Hg^{2+} (Figure 6a). Job's plot analysis at 480 nm revealed 1:1 stoichiometry between **2** and Hg^{2+}.[10] Analogous spectral trends have been observed for **1** and **3** (Figure S11−S12, Supporting Information).

A concurrent decrease in the optical density of the bands at 530 and 339 nm and an increase for the one at 480 nm with emergence of a new weak band at 393 nm occurred upon addition of Pb^{2+} (0.1 equiv) to a solution of **2**. An increase in the quantification limit of Pb^{2+} (0.2:1, 0.3:1, 0.4:1, 0.5:1, 0.6:1, 0.7:1, 0.9:1, and 1:1) leads to a gradual decrease in the optical density of the band at 530 nm (ε, 0.52×10^4 M^{-1} cm^{-1}). Simultaneously, the band at 480 nm (1.17×10^4 M^{-1} cm^{-1}) gained intensity and a new band emerged at 393 nm (0.52×10^4 M^{-1} cm^{-1}). The bands at 530 (0.36×10^4 M^{-1} cm^{-1}) and 480 nm (1.45×10^4 M^{-1} cm^{-1}) displayed substantial hypochromic and hyperchromic shifts, two new bands appeared at 701 (0.37×10^4 M^{-1} cm^{-1}) and 393 nm (0.81×10^4 M^{-1} cm^{-1}), and the color of the solution at this stage became yellowish green. Isosbestic points at 625, 496, 454, and 430 nm indicated the presence of more than two species in the medium.[10] The bands at 701, 480, and 393 nm at saturation stage (1.0 equiv, Hg^{2+}/Pb^{2+}) suggeted formation of **2**·Pb^{2+}. Job's plot analysis at 480 nm revealed 1:1 stoichiometry for **2** and Pb^{2+} (Figure 6b).[10] Analogous spectral trends have been observed for **1** and **3** in the presence of Hg^{2+}/Pb^{2+} (Figures S11 and S12, Supporting Information). Considering the similar absorption spectral behavior and color change, it is concluded that these metal ions bind to analogous interaction sites of probes **1**−**3**. Moreover, only 1.0 equiv of these cations is required by the probes to attain the saturation point. High sensitivity of the probes toward Hg^{2+}/Pb^{2+} ions is strongly suggested.

The binding affinity and sensitivity of Pd(II) complexes **4**−**6** for Hg^{2+} have also been studied by absorption titration experiments. The absorption spectral response of **4** as a function of Hg^{2+} concentration is depicted in Figure 7. Gradual addition of Hg^{2+} (0.5 equiv) to a solution of **4** (c = 10 μM; H_2O:CH_3CN, 10:90, v/v; pH ≈ 7.6) causes blue shifting of the

dx.doi.org/10.1021/ic300900m | Inorg. Chem. 2012, 51, 8916−8930

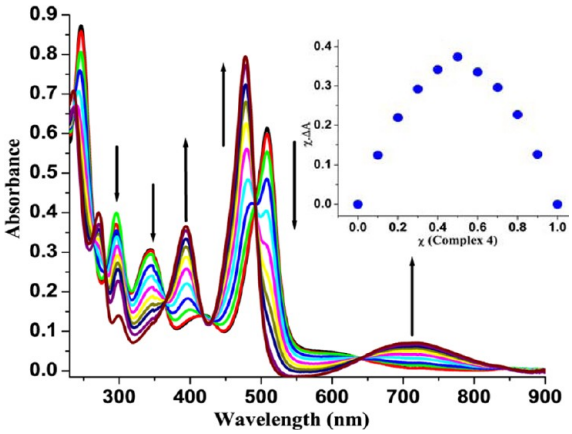

Figure 7. UV−vis spectra of **4** (c = 10 μM; H_2O:MeCN, 10:90 v/v; pH ≈ 7.6) in the presence of various amounts of Hg^{2+}. (Inset) Job's plot for **4** and Hg^{2+} indicating formation of 1:1 (**4**·Hg^{2+}) complex.

bands at 509 and 414 nm and loss of those at 343 and 294 nm. An increase in the concentration of Hg^{2+} (1.0−2.0 equiv) leads to a significant decrease in the optical density of the band at 509 nm (ε, 4.08 × 10^4 M^{-1} cm^{-1}) with the appearance of a shoulder at 477 nm (4.76 × 10^4 M^{-1} cm^{-1}). Furthermore, the band at 414 nm becomes more intense and shows a blue shift of 20 nm to appear at 394 nm. On the other hand, bands at 343 (2.37 × 10^4 M^{-1} cm^{-1}) and 293 nm (3.34 × 10^4 M^{-1} cm^{-1}) exhibited a substantial decrease in the optical density. Further addition of Hg^{2+} (2.5−5.0 equiv) leads to loss of the LE bands at 509 and 414 nm with a concomitant blue shift ($\Delta\lambda$, 32 and 20 nm, respectively) to appear as prominent bands at 477 (7.94 × 10^4 M^{-1} cm^{-1}) and 394 nm (3.56 × 10^4 M^{-1} cm^{-1}). The band at 343 nm vanished, and the one at 293 nm (1.35 × 10^4 M^{-1} cm^{-1}) exhibited a hypochromic shift. Moreover, a new prominent broad band appeared in the NIR (near-infrared) region (710 nm, 0.71 × 10^4 M^{-1} cm^{-1}), and the color of the solution turned yellowish green. Clear ratiometric isosbestic points at 641, 492, 417, and 366 nm indicated the presence of more than two species in the medium. Finally, at saturation (5.0 equiv, Hg^{2+}) four bands appeared at 710, 477, 395, and 293 nm, which have been ascribed to **4**·Hg^{2+} complex. Job's plot analysis exhibited maxima at 0.5 mol fraction, indicating 1:1 stoichiometry between **4** and Hg^{2+}. Analogous trends have been observed for **5** and **6** in the presence of Hg^{2+} (Figure S18, Supporting Information). Unlike **1**−**3**, the bands associated with the dipyrrin moiety in **4**−**6** displayed significant blue shifts in the presence of Hg^{2+}, which strongly suggested different a binding mode of palladium complexes relative to **1**−**3**. Overall, absorption studies on **1**−**6** clearly indicated the relatively high sensitivity of **1**−**3** relative to **4**−**6**.

The background presence of potentially competing cations poses a challenge in the development of a highly selective sensor for Hg^{2+} and Pb^{2+}. To explore the utility of **2** as a cation-selective chromogenic chemosensor for Hg^{2+} and Pb^{2+} competition studies have been performed and monitored by absorption spectral studies. In this direction an excess (10.0 equiv) of tested metal ions like Na^+, Ca^{2+}, Mg^{2+}, Fe^{2+}, Co^{2+}, Ni^{2+}, Cu^{2+}, Zn^{2+}, and Cd^{2+} were added to a solution containing 1.0 equiv of **2** + Hg^{2+} and **2** + Pb^{2+} (Figure 8). Interestingly, these metal ions could not alter absorption spectral features of **2** + Hg^{2+} and **2** + Pb^{2+}. Complexes **1** and **3** exhibited an analogous behavior (Figure S16, Supporting Information). Similarly, addition of an excess (10.0 equiv) of the aforesaid metal ions to a solution containing **4** + Hg^{2+} (5.0 equiv) exhibited insignificant changes (Figures 8 and S20, Supporting Information). It strongly indicated that the Hg^{2+} complex remains unaffected in a background presence of various interfering cations. Overall results strongly suggested that the selectivity of **2** for Hg^{2+}/Pb^{2+} and **4** toward Hg^{2+} is appreciable, and these may serve as a selective chromogenic chemosensor for these ions.

To gain deeper insight into the reversibility of the system an excess of a strong chelating agent like EDTA (10.0 equiv) was added to a solution of **2** + Hg^{2+}/**2** + Pb^{2+} and **4** + Hg^{2+}. Notably, addition of EDTA resulted in restitution of bands due to **2** and/or **4** (Figure S30, Supporting Information). The above observation suggested reversible interaction between **2** and Hg^{2+}/Pb^{2+} and **4** and Hg^{2+}. Regeneration of the bands may be attributed to release of Hg^{2+}/Pb^{2+} from **2** + Hg^{2+}/**2** + Pb^{2+} or **4** + Hg^{2+} and its interaction with EDTA to form a more stable EDTA−Hg/Pb complex. The above experimental observations clearly indicated that EDTA withdraws the metal ions from the probe−metal complex.

Association constants (K_a) for **1**−**3** with Hg^{2+} have been determined from the Benesi−Hildebrand method and found to be 8.98 × 10^4 (**1**), 9.49 × 10^4 (**2**), and 6.95 × 10^4 (**3**), and for Pb^{2+} these are 8.56 × 10^4 M^{-1} (**1**), 7.65 × 10^4 M^{-1} (**2**), and 7.63 × 10^4 M^{-1} (**3**). The association constants clearly supported 1:1 stoichiometry between **1**−**3** and Hg^{2+}/Pb^{2+} ions. Overall results further suggested that interaction between **1** and **2** with Hg^{2+} is stronger relative to Pb^{2+}, while **3** has a higher affinity for Pb^{2+} in comparison to Hg^{2+} under analogous conditions (Figures S13−S15, Supporting Information). It is noteworthy to mention that these changes are rapid, and a

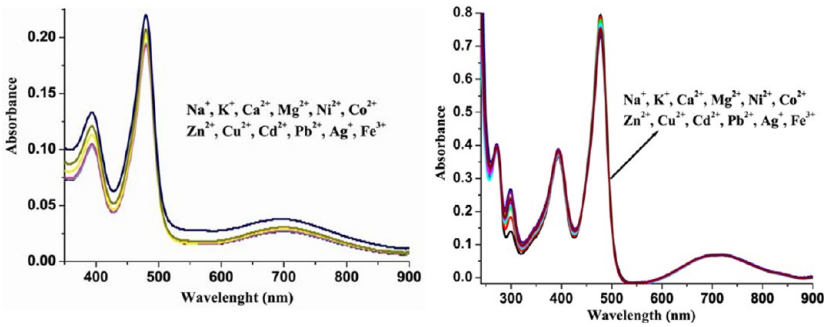

Figure 8. Evolution of the UV−vis of **2** (c = 10 μM; H_2O:EtOH, 50:50, v/v; pH ≈ 7.2) and **4** (c = 10 μM; H_2O:MeCN, 10:90 v/v; pH ≈ 7.6) in the presence of interference metal ions.

dx.doi.org/10.1021/ic300900m | Inorg. Chem. 2012, 51, 8916−8930

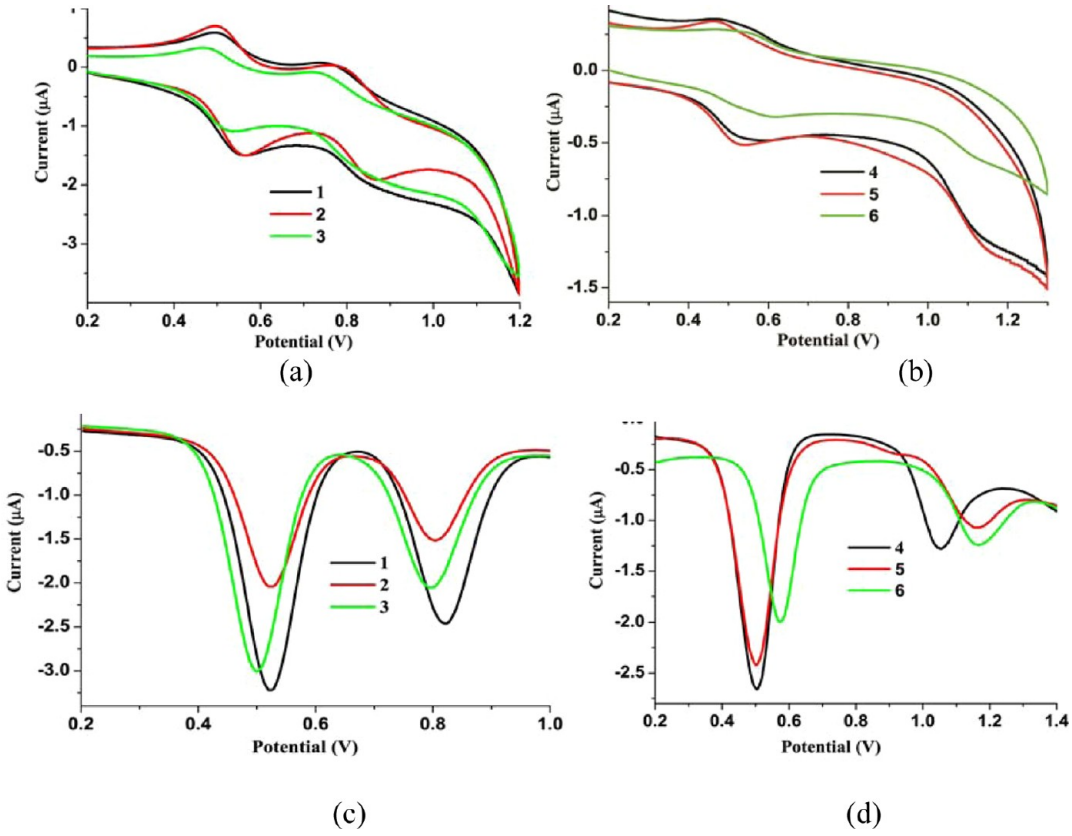

Figure 9. Cyclic voltammograms (a and b) and differential pulse voltammograms (c and d) of **1**−**6** in MeCN (c = 100 μM).

distinctive color change could be observed within 1 min. Therefore, it is concluded that the present system could find potential application in the detection of Hg^{2+} and Pb^{2+} through chromogenic response. K_a values for **4**−**6** with Hg^{2+} have also been determined (6.45 × 10^4, **4**; 6.29 × 10^4, **5**; and 6.20 × 10^4, **6**; Figure S19, Supporting Information).

The LODs for **1**−**3** are 8.12 × 10^{-7}, 7.35 × 10^{-7}, and 6.27 × 10^{-6} M for Hg^{2+} and 7.22 × 10^{-7}, 6.23 × 10^{-7}, and 5.25 × 10^{-6} M for Pb^{2+} with correlation coefficients (R^2) of 0.990, 0.993, 0.988, 0.997, 0.997, and 0.993, respectively. Further the LODs of **4**−**6** have also been determined and found to be 3.30 × 10^{-6}, 1.45 × 10^{-6}, and 1.37 × 10^{-5} M with R^2 = 0.996, 0.994, and 0.994 (Figures S21−S29, Supporting Information). The limits of detection for the complexes under investigation clearly suggest that these could find potential application in the detection of Hg^{2+}/Pb^{2+} through chromogenic response.

Electrochemical Studies. Complexes **1**−**6** possesses two redox-active units in the form of ferrocene and dithiocarbamate moieties.[16,30c,33] The interaction of metal ions through the dithiocarbamate moiety is expected to alter their redox behavior, which, in turn, can be followed by cyclic voltammetry (CV) and differential pulse voltammetry (DPV). The electrochemical cation sensing behavior of the complexes under investigation have been studied by CV and DPV in CH_3CN (c = 100 μM) using 0.1 M $[(n\text{-Bu})_4N]ClO_4$ as a supporting electrolyte at a scan rate of 50 m V s^{-1}. Resulting cyclic voltammograms and differential pulse voltammograms are depicted in Figure 9, and electrochemical data are summarized in Table S5, Supporting Information.

In their cyclic voltammograms **1**−**6** displayed distinctive oxidation double waves in the range 0.0−2.0 V. The first quasi-reversible wave (E_{pa} = 0.535, **1**; 0.538, **2**; 0.433 V, **3**; 0.448, **4**; 0.439, **5**; 0.580 V, **6**) present in these complexes has been assigned to the Fc/Fc^+ redox couple, while the other one (quasi-reversible; E_{pa} = 0.888, **1**; 0.885, **2**; 0.889 V, **3**; 1.125, **4**; 1.127, **5**; 1.119 V, **6**) has been assigned to Ni^{2+}/Ni^{3+} (**1**−**3**) and Pd^{2+}/Pd^{3+} (**4**−**6**) redox couples. The position of this wave is dependent on dtc moieties (diethyl, diisopropyl, and dibutyl) bonded to the Ni^{2+}/Pd^{2+} center. Further, in their DPV **1**−**6** exhibited oxidation peaks at E_{pa} = 0.528, **1**, 0.536, **2**, 0.496, **3**, 0.503, **4**, 0.504, **5**, and 0.575 V, **6**, assignable to the Fc/Fc^+ redox couple and 0.820, **1**, 0.805, **2**, 0.796, **3**, 1.051, **4**, 1.163, **5**, and 1.166 V, **6**, assigned to Pd^{2+}/Pd^{3+} redox couples (Figure 9).

The electrochemical sensing behavior of **1**−**3** (c = 100 μM, MeCN) toward metal ions has been investigated by CV and DPV under analogous conditions. Addition of the tested metal ions (5.0 equiv) does not show any considerable change; however, sizable changes occur only in the presence of Hg^{2+} and Pb^{2+}. To examine the sensitivity of complexes toward Hg^{2+}/Pb^{2+} electrochemical titrations have been performed. The oxidative wave due to **2** (E_{pa} = 0.885 V, Ni^{2+}/Ni^{3+}) exhibited a substantial change upon addition of 0.1 equiv of Hg^{2+}, indicating the high redox sensitivity of this complex for the said cation. Further additions of Hg^{2+} led to a gradual shift in the position of this couple to appear toward more positive potential E_{pa} 1.007 V (ΔE_{pa} = 0.122 V) with an increase in the current intensity (ΔI, 11.96%). At the same time, the wave due to the Fc/Fc^+ redox couple showed insignificant changes and addition of 1.0 equiv of Hg^{2+} led to maximum perturbations. The change in the redox couple has been ascribed to formation of **2**·Hg^{2+}.

Likewise, sequential addition of Pb^{2+} (0.0−1.0 equiv) to a solution of **2** causes a positive potential shift [Ni^{2+}/Ni^{3+}; E_{pa} 0.885 V to E_{pa}; 1.006 V; ΔE_{pa} = 0.121 V] with an increase in

dx.doi.org/10.1021/ic300900m | Inorg. Chem. 2012, 51, 8916−8930

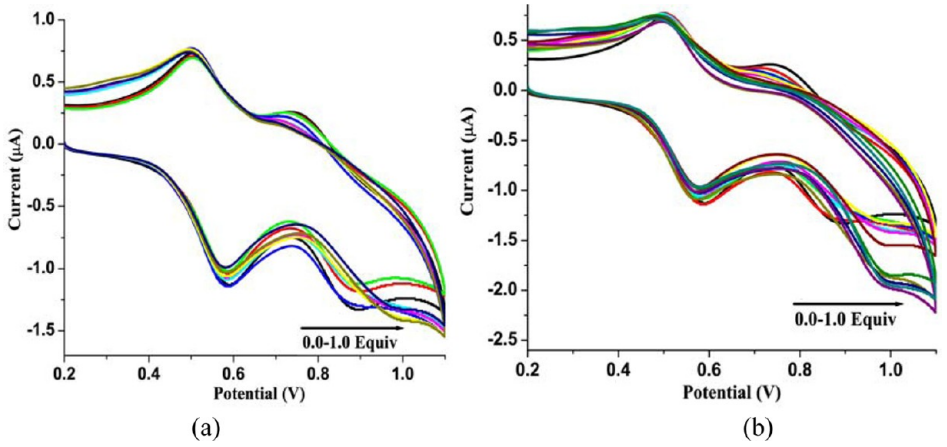

Figure 10. Cyclic voltammogram of **2** (c = 100 μM, MeCN) in the presence of (a) Hg^{2+} (c = 100 mM) and (b) Pb^{2+} (c = 100 mM) added from 0.0 to 1.0 equiv at room temperature.

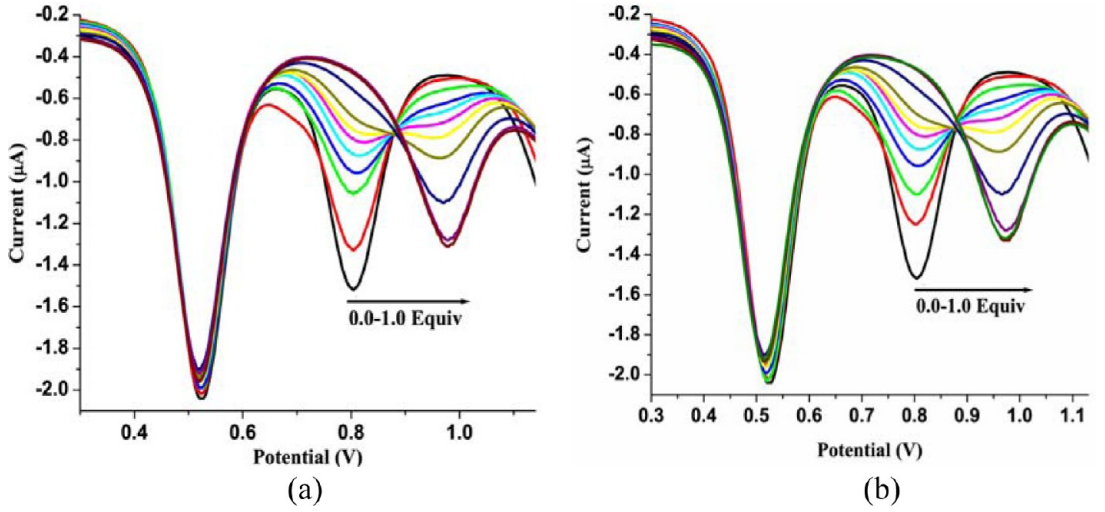

Figure 11. Evolution of the DPV of **2** (c = 100 μM, MeCN) in the presence of (a) Hg^{2+} and (b) Pb^{2+} added from 0.0 to 1.0 equiv at room temperature.

the current intensity (ΔI, 17.76%), while the oxidative wave due to Fc/Fc^{+} remains unaffected. Formation of **2**·Pb^{2+} involving interaction of Hg^{2+}/Pb^{2+} through dithiocarbamate moiety (Figure 10) is suggested. Analogous trends have been observed for **1** and **3** in the presence of Hg^{2+}/Pb^{2+} ions (Figures S32 and S33 and Table S5, Supporting Information). Further, to examine the binding site and electrochemical sensitivity DPV studies have been performed on **2** under analogous conditions. Addition of Hg^{2+} to a solution containing **2** leads to a decrease in the current intensity of the peak at E_{pa} = 0.805 V (Ni^{2+}/Ni^{3+}), with emergence of a new peak toward more positive potential at E_{pa} 0.973 V (ΔE_{pa} = 0.168 V). It may be associated with formation of a complex species. The current intensity of the new peak (E_{pa} = 0.973 V) increases with a concomitant decrease of the initial peak (Ni^{2+}/Ni^{3+}). The peak corresponding to **2** at 0.805 V (E_{pa}) completely disappeared in the presence of 1.0 equiv of Hg^{2+} (Figure 11).

Remarkably, the oxidation wave due to the Fc/Fc^{+} redox couple (E_{pa} = 0.536 V) does not show any significant alteration upon addition of Hg^{2+}. The positive potential shift of the peak due to Ni^{2+}/Ni^{3+} upon interaction with Hg^{2+} may be attributed to an electrostatic repulsion between bound metal cation and electrogenerated positive charge on the oxidized species. Thus, an appreciable shift in the redox couple (Ni^{2+}/Ni^{3+}; ΔE_{pa} = 0.168 V) suggested interaction of the metal cation with the neutral and oxidized charged probe **2**. Likewise, stepwise addition of Pb^{2+} to a solution of **2** causes a clear evolution of the oxidation peak E_{pa} = 0.805 V toward positive potential to appear at E_{pa} = 0.979 V (ΔE_{pa} = 0.174 V). The current intensity of the peak at E_{pa} = 0.805 V (Ni^{2+}/Ni^{3+}) decreases, while that for new peak at E_{pa} = 0.979 V increases. The initial peak completely disappeared and new one attained maxima in the presence of 1.0 equiv of Pb^{2+}. Notably, the oxidative response due to the Fc/Fc^{+} redox couple at E_{pa} = 0.536 V does not show a considerable change. The results obtained from DPV studies corroborated well with the one from CV. The significant positive potential shift in the oxidative response associated with the dtc moiety and negligible changes due to the Fc/Fc^{+} redox couple strongly suggested that the preferential interaction site for Hg^{2+}/Pb^{2+} is dtc not the fcdpm unit. Analogous trends have been observed for **1** and **3** in the presence of Hg^{2+}/Pb^{2+} ions, and resulting data is given in the Supporting Information (Figures S34 and S35 and Table S5).

The electrochemical sensing behavior of **4**–**6** (c = 100 μM, MeCN) toward metal ions has also been investigated by CV and DPV under analogous conditions. The studies established

dx.doi.org/10.1021/ic300900m | Inorg. Chem. 2012, 51, 8916–8930

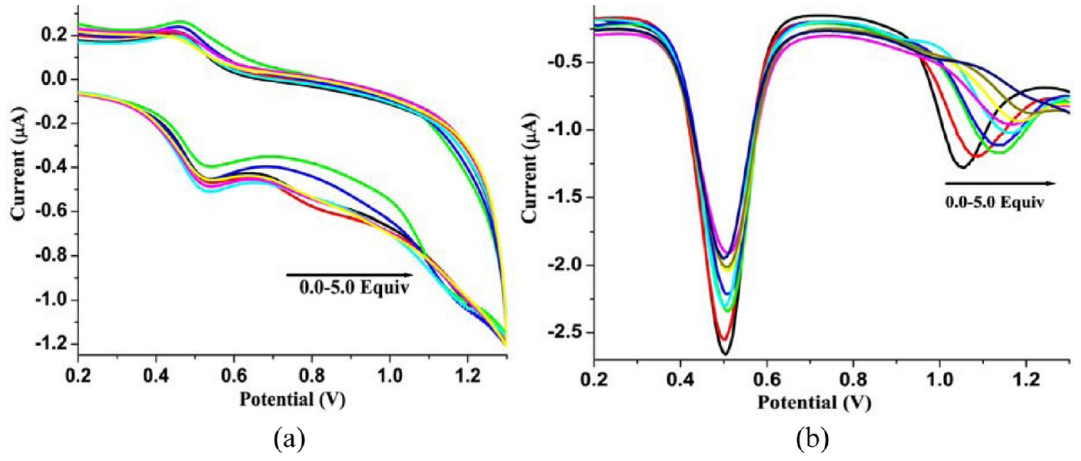

Figure 12. Evolution of the CV (a) and DPV (b) of **4** (c = 100 μM, MeCN) in the presence of Hg^{2+} (c = 100 mM) added from 0.0 to 5.0 equiv at room temperature.

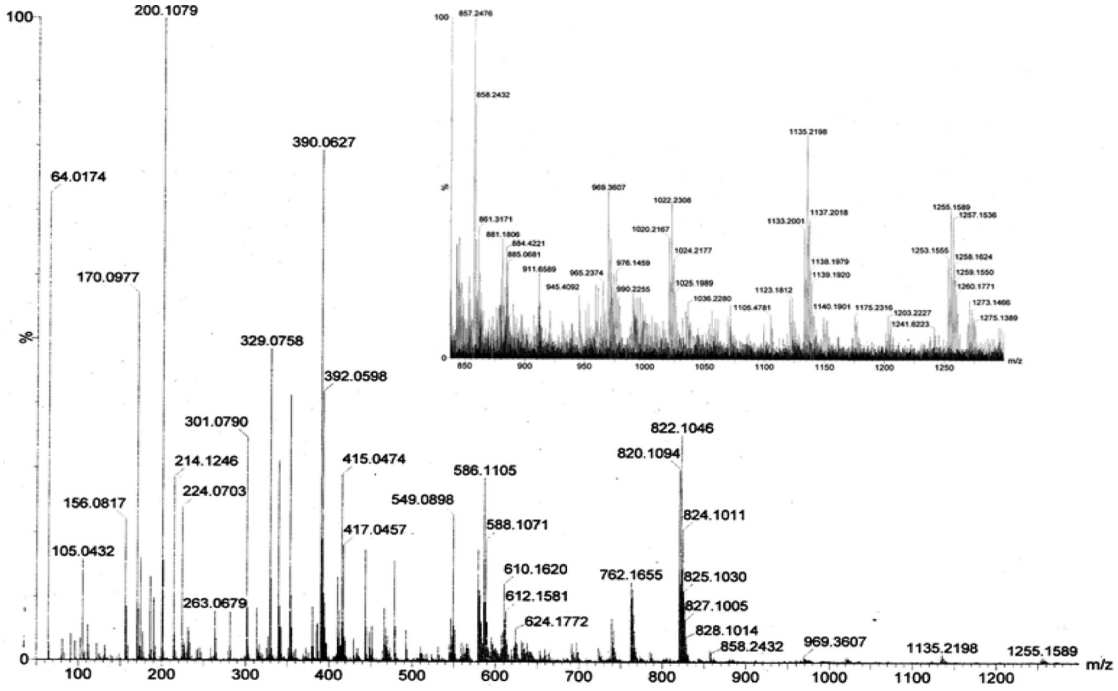

Figure 13. HRMS spectra of **2**·Hg^{2+}.

that addition of tested metal ions (5.0 equiv) does not show any significant change in CV and DPV except for Hg^{2+}. To have an idea about most probable interaction site and sensitivity of systems toward Hg^{2+} electrochemical titrations have been performed. Notably, **4**–**6** do not show appreciable changes upon addition of 0.1 equiv of Hg^{2+}. Therefore, the limit of quantification was optimized (~1.0:1.0 to 5.0:1.0). The oxidative wave due to **4** (E_{pa} = 1.125 V, Pd^{2+}/Pd^{3+}) displayed significant alteration upon addition of 1.0 equiv of Hg^{2+}. Addition of Hg^{2+} (1.5–4.0 equiv) led to a gradual positive potential shift [E_{pa} = 1.166 V (ΔE_{pa} = 0.041 V)] with a significant decrease in current intensity (ΔI, 10.27%). Addition of 5.0 equiv of Hg^{2+} causes the disappearance of the wave due to the Pd^{2+}/Pd^{3+} redox couple. It is noteworthy to mention that the wave associated with the Fc/Fc^{+} redox couple does not show any significant change; however, reversibility of the wave diminishes unlike Ni fcdpm complexes **1**–**3**. Maximum perturbation was obtained at ~5.0 equiv of Hg^{2+}, which may be ascribed to formation of **4**·Hg^{2+}. On the basis of these results we conclude that in **4**–**6** also the preferential interaction site for Hg^{2+} is the dithiocarbamate moiety, though the mode of interaction may be different (Figure 12). Analogous trends have been observed for **5** and **6** in the presence of Hg^{2+} (Figure S37 and Table S5, Supporting Information). DPV studies on **4**–**6** also supported formation of **4**·Hg^{2+} (Figures 12 and S38, Supporting Information). Overall electrochemical results suggested that interaction between the probes **1**–**3** and Hg^{2+}/Pb^{2+} is highly selective and sensitive, whereas **4**–**6** bind only with Hg^{2+} with relatively lower sensitivity.

Mass Spectral Studies. The ESI-MS of **1**–**6** displayed distinctive peaks at m/z 535.0215 (**1**, M^{+}), 561.0547 (**2**, M^{+}), 590.0918 (**3**, M + 1^{+}), 581.0001 (**4**, M^{+}), 609.0313 (**5**, M^{+}), and 637.0654 (**6**, M^{+}) (Figures S39–S46, Supporting Information). The presence of molecular ion peaks along with a peak at m/z 329 due to fcdpm in the spectra of respective complexes strongly supported their formation. To

dx.doi.org/10.1021/ic300900m | Inorg. Chem. 2012, 51, 8916–8930

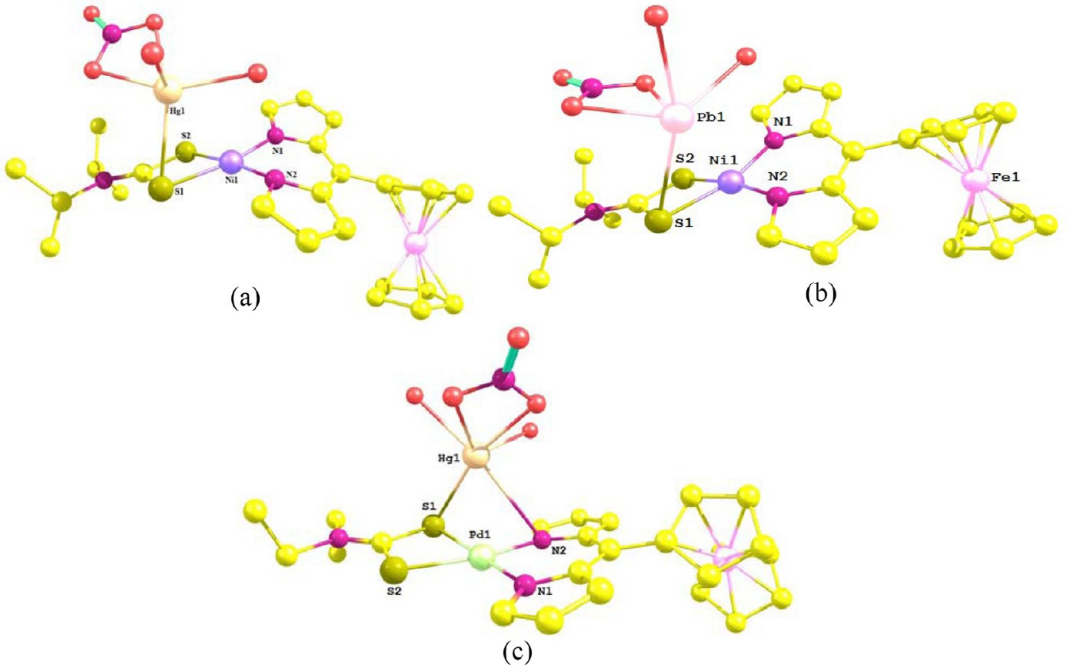

Figure 14. Calculated (6-31G**/LANL2DZ) structure for **2**+ Hg^{2+} (a), **2**+ Pb^{2+} (b), and **4**+ Hg^{2+} (c) complexes in capped sticks for clarity.

have an idea about the stoichiometry between the probes and Hg^{2+}/Pb^{2+} ions mass spectra of **7** (**2**·Hg^{2+}), **8** (**2**·Pb^{2+}), and **9** (**4**·Hg^{2+}) have been acquired. In its mass spectrum **7** exhibited prominent peaks at *m*/*z* 762.1655 and 857.2476 assignable to [**2** + Hg + **1**]$^+$ and [**2** + Hg + $2H_2O$ + NO_3^-]$^+$. On the other hand, **8** and **9** exhibited peaks at *m*/*z* 866.0954 and 881.2868 corresponding to [**2** + Pb + $2H_2O$ + NO_3^-]$^+$ and [**4** + Hg + $2H_2O$ + NO_3^-]$^+$. Observed mass spectral patterns for **7**, **8**, and **9** are quite different from those of probes **2** and **4** (Figures 13, S45, and 46, Supporting Information), and overall data is consistent with the conclusions drawn from UV–vis and electrochemical studies.

Theoretical Studies. To understand better the physicochemical phenomena of metal ion and probe interactions we carried out quantum chemical calculations. Our calculations revealed that the metal ion Hg^{2+} (or Pb^{2+}) is more likely to interact through one of the sulfur atoms of the dtc moiety in Ni–dtc complex **2** possibly because of the more soft and polarizable center. Our attempt to optimize a guess of the structure of interaction of the metal ion Hg^{2+}/Pb^{2+} with the probes in a trans arrangement indicated instability of the structure and showed us the possibility of only a 1:1 metal ion to probe interactions which has also been suggested by Job's plot analyses. Our results indicate that there are one nitrate anion, two water molecules, and one of the sulfur atoms (S1) of the dtc moiety coordinating to Hg^{2+}/Pb^{2+} to attain tetrahedral arrangement about the metal center. We started our calculations also with an initial guess structure where the metal atom is near the sulfur atom labeled as S2. Our calculation revealed that the final optimized structure converged to one in which the metal atom is close to the sulfur atom S1. This indicated a stronger interaction of the metal through sulfur atom S1, which is energetically favorable.

Geometry optimization along with frequency calculations have been performed to get insight into the proposed interaction site of the dtc moieties. Three different initial orientations of Hg^{2+} closer to that of the sulfur atoms of dtc of Pd(II) complex **4** were considered for initial guess structures. The calculations however showed that the final geometry for all calculations ended up as a single optimized structure in which Hg^{2+} interacts with the dtcs through one of the sulfur atoms and the nearest pyrrolic nitrogen atom. Optimization results suggested that there are one nitrate anion, two water molecules, a pyrrolic nitrogen, and one of the sulfur atoms of the dtc moiety coordinated to Hg^{2+} with distorted trigonal bipyramidal geometry about the metal center (Figure 14). This corroborates well to mass spectral studies.

Sensing Mechanism for Hg^{2+} and Pb^{2+}. In accordance with the Pearson's hard–soft acid–base (HSAB) concept Hg^{2+}/Pb^{2+} are soft cations and thiophilic in nature that can preferentially bind with sulfur (a soft base). Binding of **1**–**3** with Hg^{2+}/Pb^{2+} has been investigated by UV–vis, ESI-MS, and CV/DPV studies. Electronic absorption studies demonstrated ratiometric changes upon addition of Hg^{2+}/Pb^{2+} to a solution of **1**–**3** with an appreciable color change, indicating that some interaction is taking place with these cations. Significant positive potential shifts due to waves associated with Ni–dtc moieties and a negligible shift in the Fc/Fc^+ redox couple strongly suggested involvement of dtc sulfur in interaction between the probes and Hg^{2+}/Pb^{2+}. Further, ESI-MS indicated the presence of a NO_3^- and two H_2O in the resulting complex species. In **4**–**6** ratiometric changes along with a significant blue shift ($\Delta\lambda$, 32 nm) in the band associated with the dipyrrin moiety (509 nm) as well as distinct color change of the solution in the presence of Hg^{2+} indicated some interactions between **4**–**6** and Hg^{2+}; however, the binding mode may be different than that observed for **1**–**3**. Furthermore, a positive potential shift followed by the disappearance of the wave due to the Pd–dtc moiety and loss of the reversibility in the Fc/Fc^+ redox couple in electrochemical studies strongly suggested that sulfur of the dtc moieties of the receptor and nitrogen from fcdpm are involved in interaction with Hg^{2+}. It was further supported by ESI-MS, which revealed the presence of a NO_3^- and two H_2O

dx.doi.org/10.1021/ic300900m | *Inorg. Chem.* 2012, 51, 8916–8930

in the resulting complex species. The theoretical studies entirely corroborated with the experimental results (vide supra).

On the basis of overall results and theoretical studies we conclude that significant changes in the photophysical and electrochemical properties of **1**−**3** are induced by interaction of Hg^{2+}/Pb^{2+} through sulfur of the dtc moieties, whereas **4**−**6** are through a sulfur atom of the dtc moiety and one of the pyrrolic nitrogens (Figure 14). At this juncture one wonder that why these two set of complexes (Ni−fcdpm and Pd−fcdpm) exhibit different behavior. We propose that the ionic size of the respective cations ($Ni^{2+}$and Pd^{2+}) in the complexes plays an important role in determining the mode of interaction between the probes and Hg^{2+}/Pb^{2+}. As Ni^{2+} is smaller in size cations like Hg^{2+}/Pb^{2+} cannot fit well between the dtc and the fcdpm ligands to interact via dtc sulfur and pyrrolic nitrogen. In contrast, the rather large size of Pd^{2+} enables Hg^{2+} to interact through both the dtc sulfur and the pyrrolic nitrogen.

CONCLUSIONS

In summary, through the present work six novel complexes **1**−**6** containing 5-ferrocenyl-dipyrromethene and dithiocarbamates as auxiliary ligands have been synthesized and used as a multichannel (chromogenic, electrochemical) chemosensor for Hg^{2+} and Pb^{2+}. The Ni−fcdpm complexes **1**−**3** exhibited distinct naked-eye change from brown to yellowish green in the presence of Hg^{2+} and Pb^{2+}, while those based on palladium (**4**−**6**) was only in the presence of Hg^{2+} over other metal cations. Interaction between Hg^{2+}/Pb^{2+} and sulfur of dithiocarbamates is responsible for significant variation in optical and electrochemical signals of **1**−**3**, whereas binding of one of the pyrrolic nitrogens and dtc sulfur with Hg^{2+} in **4**−**6** may be attributed to the ionic size of the metal centers (Ni^{2+} and Pd^{2+}). To the best of our knowledge, this is the first report dealing with a chemosensor for any transition/heavy metal ion based on complexes incorporating fcdpm dithiocarbamates as ancillary ligand. Preliminary understanding of the Hg^{2+}/Pb^{2+} sensing mechanism would help in designing new series of complexes containing both fcdpm and dithiocarbamates by simply modifying the chemical structure of ligands to contain specific coordinating sites and explore their potential applications, especially as chemosensors. We believe that our results and elaborations may provide a useful and pioneering guide to designing new complexes containing dipyrrins and dithiocarbamates as coligands.

ASSOCIATED CONTENT

Supporting Information

^1H and ^{13}C NMR results, UV−vis titration curves, CV and DPV, HRMS, and motifs resulting from various weak bonding interactions. This material is available free of charge via the Internet at http://pubs.acs.org. CCDC deposition Nos. 856055 (**1**), 856056 (**2**), 868304 (**4**), and 868305 (**5**) contain supplementary crystallographic data for this paper.

AUTHOR INFORMATION

Corresponding Author

*Phone + 91 542 6702480. Fax: + 91 542 2368174. E-mail: dspbhu@bhu.ac.in.

Notes

The authors declare no competing financial interest.

ACKNOWLEDGMENTS

The authors thank the Council of Scientific and Industrial Research, New Delhi, for financial assistance through Scheme HRDG 01 (2361)/10/EMR-II) and for the award of a Junior Research Fellowship to R.K.G. (No. 09/013(0210)/2009-EMR-I). We are also thankful to the Head, Department of Chemistry, Faculty of Science, Banaras Hindu University, Varanasi (U.P.), India, for extending laboratory facilities, National Institute of Advanced Industrial Science and Technology (AIST), Osaka, Japan, and National Institute of Science and Educational Research (NISER) for extending the single-crystal X-ray facility.

REFERENCES

(1) (a) In *Fluorescent Chemosensors for Ion and Molecule Recognition*; Czarnik, A. W., Ed.; American Chemical Society: Washington, DC, 1993; p 1. (b) de Silva, A. P.; Gunaratne, H. Q. N.; Gunnlaugsson, T.; Huxley, A. J. M.; McCoy, C. P.; Rademacher, J. T.; Rice, T. E. *Chem. Rev.* **1997**, *97*, 1515.

(2) (a) Tchounwou, P. B.; Ayensu, W. K.; Ninashvili, N.; Sutton, D. *Environ. Toxicol.* **2003**, *18*, 149. (b) Harris, H. H.; Pickering, I. J.; George, G. N. *Science* **2003**, *301*, 1203. (c) Von, B. R. *J. Appl. Toxicol.* **1995**, *15*, 483. (d) Gutknecht, J. *J. Membr. Biol.* **1981**, *61*, 61.

(3) (a) Von, R. B.; Greenwood, M. R. In *Metals and Their Compounds in the Environment*; Merian, E., Ed.; VCH: Weinheim, 1991; p 1045. (b) Wu, D.; Huang, W.; Lin, Z.; Duan, C.; He, C.; Wu, S.; Wang, D. *Inorg. Chem.* **2008**, *47*, 7190. (c) Basu, N.; Schouhammer, A.; Grochowina, N.; Klenavic, K.; Evans, D.; Brien, M. O.; Chan, M. *Environ. Sci. Technol.* **2005**, *39*, 3585.

(4) (a) Aspmo, K.; Temme, C.; Berg, T.; Ferrari, C.; Gauchard, P. A.; Fain, X.; Wibetoe, G. *Environ. Sci. Technol.* **2006**, *40*, 4083. (b) *Capsule Report: Aqueous Mercury Treatment; Office of Research and Development*; U.S. EPA: Washington, DC, 1997. (c) Coronado, E.; Mascaros, J. R. G.; Gastaldo, C. M.; Palomares, E.; Durrant, J. R.; Vilar, R.; Gratzel, M.; Nazeeruddin, M. K. *J. Am. Chem. Soc.* **2005**, *127*, 12351.

(5) (a) Miller, J. R.; Rowland, J.; Lechler, P. J.; Desilets, M.; Hsu, L. C. *Water, Air, Soil Pollut.* **1996**, *86*, 373. (b) Huang, J.; Xu, Y.; Qian, X. *J. Org. Chem.* **2009**, *74*, 2167. (c) Guliyev, R.; Coskun, A.; Akkaya, E. U. *J. Am. Chem. Soc.* **2009**, *131*, 9007. (d) Wu, D. Y.; Huang, W.; Lin, Z. H.; Duan, C. Y.; He, C.; Wu, S.; Wang, D. H. *Inorg. Chem.* **2008**, *47*, 7190. (e) Pacyna, E. G.; Pacyna, J. M.; Steenhuisen, F.; Wilson, S. *Atmos. Environ.* **2006**, *40*, 4048. (f) Tchounwou, P. B.; Ayensu, W. K.; Ninashvili, N.; Sutton, D. *Environ. Toxicol.* **2003**, *18*, 149. (g) Clarkson, T. W.; Magos, L.; Myers, G. J. *N. Engl. J. Med.* **2003**, *349*, 1731.

(6) Alfonso, M; Tarraga, A; Molina, P. *J. Org. Chem.* **2011**, *76*, 939 and references therein..

(7) (a) Fu Lin, J. S. Lead Poisoning, A Century of Discovery and Rediscovery. In *Human Lead Exposure*; Needleman, H. L., Ed.; Lewis Publishing: Boca Raton, FL, 1992.

(8) (a) Aragay, G.; Pons, J.; Merkoci, A. *Chem. Rev.* **2011**, *111*, 3433. (b) Zhao, Q.; Li, F.; Huang, C. *Chem. Soc. Rev.* **2010**, *39*, 3007. (c) Lau, Y. H.; Rutledge, P. J.; Watkinson, M.; Todd, M. H. *Chem. Soc. Rev.* **2011**, *40*, 2848.

(9) (a) Rivas, R. E.; Lopez-Garcia, I.; Hernandez-Cordobo, M. *Anal. Methods* **2010**, *2*, 225. (b) Dallali, N.; Zahedi, M. M.; Yamimi, Y.; Agrawal, Y. K. *Rev. Anal. Chem.* **2009**, *28*, 125. (c) Skrzydlewska, E; Balcerzak, M; Vanhaecke, F *Anal. Chim. Acta* **2003**, *479*, 191. (d) Grindlay, G.; Mora, J.; Gras, L.; de Loos-Vollebregt, M. T. C. *Anal. Chim. Acta* **2009**, *652*, 154.

(10) (a) Zhao, Y.; Zhong, Z. Q. *J. Am. Chem. Soc.* **2006**, *128*, 9988. (b) Lin, S. Y.; Wu, S. M.; Chen, C. H. *Angew. Chem., Int. Ed.* **2006**, *45*, 4948. (c) Tatay, S.; Gavina, P.; Coronado, E.; Palomares, E. *Org. Lett.* **2006**, *8*, 3857. (d) Caballero, A.; Lloveras, V.; Curiel, D.; Tarraga, A.; Espinosa, A.; Garcıa, R.; Vidal-Gancedo, J.; Rovira, C.; Wurst, K.; Molina, P.; Veciana, J. *Inorg. Chem.* **2007**, *46*, 825. (e) Wu, D.; Huang, W.; Lin, Z.; Duan, C.; He, C.; Wu, S.; Wang, D. *Inorg. Chem.* **2008**, *47*, 7190. (f) Huang, W.; Song, C.; He, C.; Lv, G.; Hu, X.; Zhu, X.; Duan,

C. *Inorg. Chem.* **2009**, *48*, 5061. (g) Chen, X.; Nam, S. W.; Jou, M. J.; Kim, Y.; Kim, S. J.; Park, S.; Yoon, J. *Org. Lett.* **2008**, *10*, 5235.
(11) (a) Gunnlaugsson, T.; Leonard, J. P.; Murray, N. S. *Org. Lett.* **2004**, *6*, 1557. (b) Zhou, Y.; Won, J.; Lee, J. Y.; Yoon, J. *Chem. Commun.* **2011**, *47*, 1997. (c) Quinlan, E.; Matthews, S. E.; Gunnlaugsson, T. *J. Org. Chem.* **2007**, *72*, 7497. (d) Maity, D.; Govindaraju, T. *Chem. Commun.* **2010**, *46*, 4499.
(12) (a) Xie, Z.; Wang, K.; Zhang, C.; Yang, Z.; Chen, Y.; Guo, Z.; Lua, G. Y.; He, W. *New J. Chem.* **2011**, *35*, 607. (b) Zapata, F.; Caballero, A.; Molina, P.; Tarraga, A. *Sensors* **2010**, *10*, 11311.
(13) (a) Wood, T. E.; Thompson, A. *Chem. Rev.* **2007**, *107*, 1831. (b) Baudron, S. A. *CrystEngComm* **2010**, *12*, 2288.
(14) (a) Wagner, R. W.; Lindsey, J. S. *J. Am. Chem. Soc.* **1994**, *116*, 9759. (b) Koepf, M.; Trabolsi, A.; Elhabiri, M.; Wytko, J. A.; Paul, D.; Gary, A. M. A.; Weiss, J. *Org. Lett.* **2005**, *7*, 1279. (c) Maeda, H.; Hasegawa, M.; Hashimoto, T.; Kakimoto, T.; Nishio, S.; Nakanishi, T. *J. Am. Chem. Soc.* **2006**, *128*, 10024. (d) Hall, J. D.; McLean, T. M.; Smalley, S. J.; Waterland, M. R.; Telfer, S. G. *Dalton Trans.* **2010**, *39*, 437.
(15) (a) Latorre, A.; Urbano, A.; Carreño, M. C. *Chem. Commun.* **2011**, *47*, 8103. (b) Sadhukhan, N.; Bera, J. K. *Inorg. Chem.* **2009**, *48*, 978.
(16) (a) Beer, P. D.; Gale, P. A.; Chen, G. Z. *Coord. Chem. Rev.* **1999**, *3*, 185. (b) Staveren, D. R. V.; Nolte, N. M. *Chem. Rev.* **2004**, *104*, 5931. and references therein. (c) Metzler-Nolte, N. *Angew. Chem., Int. Ed.* **2001**, *40*, 1040.
(17) (a) Molina, P.; Tarraga, A.; Caballero, A. *Eur. J. Inorg. Chem.* **2008**, 4301. (b) Zapata, F.; Caballero, A.; Espinosa, A.; Tarraga, A.; Molina, P. *J. Org. Chem.* **2009**, *74*, 4787. (c) Zapata, F.; Caballero, A.; Espinosa, A.; Tarraga, A.; Molina, P. *Inorg. Chem.* **2009**, *48*, 11566. (d) Romero, T.; Caballero, A.; Tarraga, A.; Molina, P. *Org. Lett.* **2009**, *11*, 3466. (e) Zapata, F.; Caballero, A.; Espinosa, A.; Tarraga, A.; Molina, P. *Dalton Trans.* **2010**, *39*, 5429.
(18) Pearson, R. G. *J. Am. Chem. Soc.* **1963**, *85*, 3533.
(19) (a) Zhao, Q.; Cao, T.; Li, F.; Li, X.; Jing, H.; Yi, T.; Huang, C. *Organometallics* **2007**, *26*, 2077. (b) Zhao, Q.; Liu, S.; Li, F.; Yi, T.; Huang, C. *Dalton Trans.* **2008**, 3836. (c) Chen, Y.; Sun, Z. H.; Song, B. E.; Liu, Y. *Org. Biomol. Chem.* **2011**, *9*, 5530. (d) Tan, J.; Yan, X. P. *Talanta* **2008**, *76*, 9. (e) Cheng, X.; Li, Q.; Qin, J.; Li, Z. *Appl. Mater. Interface* **2010**, *2*, 1066.
(20) (a) Yadav, M.; Singh, A. K.; Pandey, D. S. *Organometallics* **2009**, *28*, 4713. (b) Yadav, M.; Singh, A. K.; Maiti, B.; Pandey, D. S. *Inorg. Chem.* **2009**, *48*, 7593−9929. (c) Yadav, M.; Kumar, P.; Singh, A. K.; Ribas, J.; Pandey, D. S. *Dalton Trans.* **2009**, 9929. (d) Yadav, M.; Kumar, P.; Pandey, D. S. *Polyhedron* **2010**, *29*, 791. (e) Yadav, M.; Singh, A. K.; Pandey, D. S. *J. Organomet. Chem.* **2011**, *696*, 758. (f) Gupta, R. K.; Yadav, M.; Pandey, R.; Pandey, D. S. *J. Chem. Sci.* **2011**, *123*, 819.
(21) Perrin, D. D.; Armango, W. L. F.; Perrin, D. R. *Purification of laboratory Chemicals*; Pergamon: Oxford, U.K., 1986.
(22) (a) Auger, A.; Swarts, J. C. *Organometallics* **2007**, *26*, 102. (b) Auger, A.; Muller, A. J.; Swarts, J. C. *Dalton Trans.* **2007**, 3623. (c) Nemykin, V. N.; Galloni, P.; Floris, B.; Barrett, C. D.; Hadt, R. G.; Subbotin, R. I.; Marrani, A. G.; Zanoni, R.; Loim, N. M. *Dalton Trans.* **2008**, 4233. (d) Gallagher, J. F.; Moriarty, E. *Acta Crystallogr., Sect. C* **1999**, *55*, 1079.
(23) (a) Sheldrick, G. M. *SHELXL-97, Program for X-ray Crystal Structure Refinement*; Göttingen University: Göttingen, Germany, 1997. (b) Sheldrick, G. M. *SHELXS-97, Program for X-ray Crystal Structure Solution*; Göttingen University: Göttingen, Germany, 1997.
(24) (a) Spek, A. L. *PLATON, A Multipurpose Crystallographic Tools*; Utrecht University: Utrecht, The Netherlands, 2000. (b) Spek, A. L. *Acta Crystallogr., Sect. A* **1990**, *46*, C31.
(25) Pandey, R.; Gupta, R. K.; Shahid, M.; Maiti, B.; Misra, A.; Pandey, D. S. *Inorg. Chem.* **2012**, *51*, 298.
(26) (a) Bartolottiand, L. J.; Fluchick, K. In *Reviews in Computational Chemistry*; Lipkowitz, K. B., Boyd, D., Eds.; VCH: New York, 1996; Vol. 7, pp 187−216. (b) Becke, A. D. *J. Chem. Phys.* **1993**, *98*, 5648. (c) Lee, C. T.; Yang, W. T.; Parr, R. G. *Phys. Rev. B* **1988**, *37*, 785. (d) Hay, P.; Wadt, W. R. *J. Chem. Phys.* **1985**, *82*, 270. (e) Frisch, M. J.; et al. *Gaussian 03*, Revision E.01; Gaussian, Inc.: Wallingford, CT, 2007.
(27) (a) Birri, A.; Harvey, B.; Hogarth, G.; Subasi, E.; Ugur, F. *J. Organomet. Chem.* **2007**, *692*, 2448. (b) Blake, A. J.; Kathirgamanathan, P.; Toohey, M. J. *Inorg. Chim. Acta* **2000**, *303*, 137.
(28) (a) Skibar, W.; Kopacka, H.; Wurst, K.; Salzmann, C.; Ongania, K. H.; Biani, F. F.; Zanello, P.; Bildstein, B. *Organometallics* **2004**, *23*, 1024. (b) Malachowski, M. R.; Grau, M. F.; Thomas, J. M.; Rheingold, A. L.; Moore, C. E. *Inorg. Chim. Acta* **2010**, *364*, 132.
(29) Pogozhev, D.; Baudron, S. A.; Hosseini, M. W. *CrystEngComm* **2010**, *12*, 2238. (b) Gill, H. S.; Finger, I.; zidarevic, I. B.; Szydlo, F.; Scott, M. J. *New J. Chem.* **2005**, *29*, 68.
(30) (a) Husain, A.; Nami, S. A. A.; Singh, S. P.; Oves, M.; Siddiqi, K. S. *Polyhedron* **2011**, *30*, 33. (b) Fackler, J. P.; Avdeef, A.; Fischer, R. G. *J. Am. Chem. Soc.* **1973**, *95*, 774. (c) Harding, D. J.; Harding, P.; Dokmaisrijana; Adams, S. H. *Dalton Trans.* **2011**, *40*, 1313.
(31) (a) Bronner, C.; Baudron, S. A.; Hosseini, M. W.; Strassert, C. A.; Guenetb, A.; Cola, L. D. *Dalton Trans.* **2010**, *39*, 180. (b) Gupta, R. K.; Pandey, R.; Sharma, S.; Pandey, D. S. *Dalton Trans.* **2012**, *41*, 8556.
(32) Desiraju, G. R.; Steiner, T. *The Weak Hydrogen Bond in Structural Chemistry and Biology*; Oxford University Press: Oxford, 1999.
(33) (a) Eckermann, A. L.; Shaw, J. A.; Meade, T. J. *Langmuir* **2010**, *26*, 2904. (b) Giovagnini, L.; Sitran, S.; Montopoli, M.; Caparrotta, L.; Corsini, M.; Rosani, C.; Zanello, P.; Dou, Q. P.; Fregona, D. *Inorg. Chem.* **2008**, *47*, 6336.